

Recent advances in application of transition metal phosphides for photocatalytic hydrogen production

Yang Yang, Chengyun Zhou, Wenjun Wang, Weiping Xiong, Guangming Zeng*, Danlian Huang*,
Chen Zhang*, Biao Song, Wenjing Xue, Xiaopei Li, Ziwei Wang, Donghui He, Hanzhuo Luo,
Zenglin Ouyang

*College of Environmental Science and Engineering, Hunan University and Key Laboratory of
Environmental Biology and Pollution Control (Hunan University), Ministry of Education,
Changsha 410082, P. R. China*

Accepted MS

* Corresponding authors at: College of Environmental Science and Engineering, Hunan University, Changsha, 410082, PR China.

E-mail addresses: zgming@hnu.edu.cn (G. Zeng), huangdanlian@hnu.edu.cn (D. Huang) and zhangchen@hnu.edu.cn (C. Zhang).

Abstract

Searching a sustainable way to efficiently produce hydrogen (H_2) is critical to realizing the “hydrogen economy”, which may resolve the global energy and environmental issues nowadays. The conversion of solar energy to hydrogen energy based on photocatalytic water splitting is an ideal technology for environmental-friendly and economically producing H_2 . Exploring high-performance and earth-abundant cocatalysts that can replace noble metal-based cocatalysts is essential to achieving highly efficient and cost-effective photocatalytic H_2 production. In recent years, transition metal phosphides (TMPs) have been regarded as promising candidates to replace noble metal-based cocatalysts for photocatalytic H_2 production. This review presents a panorama of the latest progress in the developments of TMPs for photocatalytic H_2 production. Concretely, this review starts with the functions of TMPs in photocatalytic H_2 production, followed by the synthetic strategies of TMPs and the loading methods of TMPs on semiconductors. Then the application and mechanism of the common TMPs in photocatalytic H_2 production are discussed in detail, including iron phosphides, cobalt phosphides and nickel phosphides. Lastly, we provide a comprehensive conclusion and outlook on the major challenges and opportunities for better developments in the future research. It is reasonable to believe that the TMPs is a rising star in photocatalytic H_2 production.

Keywords: transition metal phosphides; cocatalyst; photocatalysis; H_2 production

1. Introduction

The growing consumption of energy and the consequent climate changes as well as environmental problems make it urgent to seek renewable and environment-friendly alternative energy sources to fossil fuels [1-5]. H_2 is considered as the most development potential candidate for the future energy supply owing to its high gravimetric energy density and calorific value, as well as clean combustion product (H_2O) [6-8]. At present, the main industrial method is H_2 production from fossil resources, including gasification of coal, steam reforming of natural gas and partial oxidation of hydrocarbons [9-11]. Although a considerable amount of H_2 can be produced at low cost in these processes, the consumption of fossil resources will lead to the greenhouse gas emission. Thus, developing a green, sustainable and efficient strategy for H_2 production is imperatively required.

Since Fujishima et al. [12] developed the photoelectrochemical water splitting on a rutile TiO_2 anode in 1972, photocatalytic water splitting using semiconductor photocatalysts has become a promising technology to convert solar energy into hydrogen energy [13, 14]. This is an environmental-friendly technology as H_2 can be produced through the interaction among solar light, photocatalyst and water in this process. Moreover, the easy synthesis of photocatalysts and the facile design of photoreactors make photocatalytic water splitting a low cost technology with the potential for large scale H_2 production [15, 16]. A technical/economic analysis has demonstrated that when some photoreactors were operated with a solar-to-hydrogen (STH) energy conversion efficiency of 5-10%, photocatalytic water splitting was economically feasible for the H_2 production [17, 18]. As displayed in Fig. 1a, the number of publications related to photocatalytic H_2 production shows an exponential growth trend. Generally, the photocatalytic H_2 production reaction includes three main steps: (i) semiconductor absorbs light to generate electron-hole pairs, (ii) photogenerated electron-hole pairs are separated and transferred to the surface of semiconductor, and (iii) H_2 evolution on the

surface of semiconductor (Fig. 2). The relative balance of kinetics and thermodynamics of these three steps influences the efficiency of photocatalytic H₂ production. Therefore, many efforts have been paid to construct novel photocatalysts with broad absorption spectrum and efficient charge separation and transfer in the last few decades [19-21]. For example, some novel photocatalysts with narrow bandgap have been developed, such as Ag₃PO₄, Bi₂WO₆ and g-C₃N₄ [22-25]. Meanwhile, in order to improve the light harvesting ability of wide bandgap photocatalysts, a variety of strategies have also been exploited, such as heterojunction construction [26, 27], plasmonic metals coupling [28], dye sensitization [29], doping [30] and defect engineering [31]. In addition, various nanostructured photocatalysts have been designed to shorten charge diffusion length, thus achieving highly efficient charge separation and transfer [32]. Moreover, the heterojunction construction [33, 34], doping [35, 36] and defect engineering [37] are also widely employed to accelerate the charge separation and transfer.

In the last decades, cocatalysts loading has stimulated much attention as it can not only enhance the light harvesting and assist charge transfer but also provide reaction active sites and improve photocatalysts stability [38, 39]. Thus, cocatalysts play an important role for enhancing both the activity and stability of photocatalysts [40-42]. Among the various cocatalysts, noble metal-based cocatalysts have been extensively studied as highly active cocatalysts toward photocatalytic H₂ production, such as Pt, Pd, Au, Ag, Ru and Rh [43, 44]. Nevertheless, the scarcity and accompanying expensive price limit the large scale application of these noble metal-based cocatalysts (Table 1). Accordingly, the development of noble metal free cocatalysts with low cost and high efficiency is urgently demanded for photocatalytic H₂ production. Recently, earth-abundant transition metal phosphides (TMPs) have been recognized as affordable and efficient catalysts for hydrogen evolution reaction (HER) and have drawn increasing attention (Fig. 1b). As early as in 2005, Liu et al. [45]

predicted that Ni_2P was a highly active HER catalyst using density functional theory (DFT) calculations. In 2013, Xu et al. [46] first reported that FeP had excellent activity in electrochemical H_2 evolution. Since Cao et al. [47] first demonstrated that Ni_2P was an outstanding cocatalyst for photocatalytic H_2 production in 2014, many efforts have been devoted to introducing TMPs into photocatalytic H_2 production system [48-52].

Because many achievements have been made in developing TMPs cocatalysts for photocatalytic H_2 production in recent years, it is necessary to summarize the recent progresses and thus promote further developments of this field. In this review, we summarize the recent advances of TMPs in photocatalytic H_2 production. Firstly, the functions of TMPs in photocatalytic H_2 production are discussed. Then, the synthetic strategies of TMPs and the loading methods of TMPs on semiconductors are introduced. Next, the applications and mechanisms of the common TMPs in photocatalytic H_2 production are stated. Finally, the challenges and opportunities of TMPs in photocatalytic H_2 production are proposed.

2. Functions of TMPs in photocatalytic H_2 production

In photocatalytic H_2 production, the TMPs cocatalysts play significant roles in promoting both the activity and stability of semiconductor photocatalysts, mainly including enhancing light absorption, providing active sites, accelerating charge transfer, lowering overpotential and strengthening photostability.

2.1. Enhance light absorption

Light harvesting capability is an important factor influencing photocatalytic activity because the enhanced light absorption ability can improve the utilization efficiency of solar energy [53]. TMPs have been reported to effectively enhance the light absorption due to their dark appearance. For example, in the study of Zhao et al. [54], the pure Fe_xP presented an intense absorption in the

wavelength range from 350 to 800 nm, while the absorption edge of pure g-C₃N₄ located at approximately 450 nm. After introducing Fe_xP into g-C₃N₄, although the absorption edge of Fe_xP/g-C₃N₄ did not change significantly compared to g-C₃N₄, an enhanced light absorption was observed in Fe_xP/g-C₃N₄ in the wavelength range from 450 to 800 nm, which was ascribed to the high visible light absorption ability of Fe_xP. Huang et al. [55] found that the pristine CoP₃ possessed an efficient absorption from the visible light to near-infrared light region because of its narrow band gap. Benefiting from the intrinsic absorption of black-colored CoP₃, the CoP₃/Mn_{0.2}Cd_{0.8}S nanocomposite exhibited enhanced light absorption. Moreover, the Ni₂P, Ni₁₂P₅ and Ni₃P could also efficiently enhance the light absorption of g-C₃N₄ because of their dark color [56]. Accordingly, the TMPs cocatalysts can significantly enhance the light absorption, which will promote the generation of more available photogenerated electrons to participate in the photocatalytic H₂ production.

2.2. Provide active sites

Constructing surface active sites to achieve rapid charge transfer and effective water molecule adsorption is beneficial to improve the performance of the photocatalyst for photocatalytic H₂ production [57]. TMPs can provide abundant active sites and push forward photocatalytic H₂ production. For example, in the CoP/g-C₃N₄ composite, a large number of photogenerated electrons transferred from g-C₃N₄ to the surface CoP catalytic active sites under visible light irradiation [58]. Then the enriched electrons on CoP reacted with adsorbed protons to produce H₂. Thus, CoP could act as the electron sink and provide effective proton reduction sites to promote H₂ production. Moreover, both metal atom and P atom in TMPs can be active sites. Li et al. [59] revealed that the P(δ⁻)-Co(δ⁺)-N(δ⁻) bonding state was formed among P, Co, and N atoms in tertiary nitrogen groups on the interface of CoP and g-C₃N₄. The Co(δ⁺)-N(δ⁻) bonds could stabilize the CoP cocatalyst on the surface of g-C₃N₄, promote the photogenerated charge carrier separation and transfer, and regulate

the CoP activity. Meanwhile, the $P(\delta^-)-Co(\delta^+)$ bonds were favorable to the formation of high electron density protonated $P(\delta^-)$ pendant moieties and Co-hydride, which made the adjacent P and Co atoms serve as dual proton adsorption sites to accelerate the photocatalytic H_2 production from water.

2.3. Accelerate charge transfer

The transfer behavior of photogenerated charge carriers is a significant factor affecting the photocatalytic activity. TMPs cocatalysts can accelerate interfacial charge transfer at the interface of TMPs and semiconductors due to their intrinsic metallicity [60, 61]. When TMPs is loaded on the surface of semiconductors, a close contact can be established between their interfaces, which leads to the formation of heterojunction, hence accelerating the separation and transfer of photogenerated electron-hole pairs. As depicted in Fig. 3, the photogenerated electrons on the conduction band (CB) of a semiconductor will migrate to the TMPs and reduce protons to H_2 molecules. In general, the relative energy level between semiconductor and TMPs determines the direction and efficiency of the charge transfer [43]. In the study of Wang et al. [62], the Fermi level of CoP was determined to be lower than that of g- C_3N_4 . When CoP was loaded on the surface of g- C_3N_4 , the free electrons would transfer from g- C_3N_4 to CoP until the Fermi levels were aligned, which would induce the formation of built-in electric field oriented from g- C_3N_4 towards CoP. Therefore, under visible light irradiation, the photogenerated electrons on g- C_3N_4 would be directionally transferred to CoP to produce H_2 . He et al. [63] discovered that the Ni_2P could be used as an interface electronic bridge to link the two conduction bands of g- C_3N_4 and CdS for facilitating the transfer of photogenerated charge carriers. DFT calculations demonstrated that the work functions of g- C_3N_4 , Ni_2P and CdS were 4.23, 4.52 and 5.18 eV, respectively. Accordingly, the Fermi level was g- C_3N_4 , Ni_2P and CdS in descending order. During photocatalytic H_2 production, the photogenerated electrons migrated from g- C_3N_4 to Ni_2P and CdS or migrated from Ni_2P to CdS, resulting in the formation of built-in electric field, thereby

efficiently promoting the separation and transfer of photogenerated charge carriers. Compared to CdS/g-C₃N₄, the photoluminescence (PL) intensity of CdS/Ni₂P/g-C₃N₄ was decreased, implying the positive role of Ni₂P on the charge carrier dynamics. Moreover, Lin et al. [64] reported that the appropriate charge transfer distance between the semiconductor and TMPs was also a key factor for accelerating charge transfer. In short, the TMPs cocatalysts can efficiently accelerate charge transfer and enable more photogenerated electrons to get involved in the process of H₂ production.

2.4. Lower overpotential

Overpotential is the difference between the thermodynamically determined reduction potential and the experimental potential, which is mainly used to overcome the inherent activation energy barrier during electrode reaction and the resistance consumption [50, 65]. However, in the process of photocatalytic water splitting, semiconductors always have a high surface overpotential for HER, resulting in the decrease of reaction rate and the loss of energy [66, 67]. It has been found that TMPs cocatalysts could efficiently lower the overpotential for HER on the surface of semiconductors. In the study of Zhen et al. [68], the overpotential of CdS, Ni₂P, Pt@CdS and Ni₂P@CdS were determined to be -0.53, -0.38, -0.34 and -0.32 V vs. saturated calomel electrode (SCE), respectively. Among these, the Ni₂P@CdS possessed the lowest overpotential, which might be ascribed to the fast transfer of electrons. Accordingly, the Ni₂P@CdS exhibited excellent photocatalytic performance for H₂ production due to the low overpotential for HER. Sun et al. [69] reported that the Fe₂P, Co₂P and Ni₂P could all cause a negative shift of onset potential for g-C₃N₄. The negative shift of onset potential indicated the reduced overpotential, which was beneficial to the photocatalytic H₂ production. Normally, the photocatalyst with lower overpotential requires less energy to obtain the same photocurrent density. In the study of Bi et al. [70], when the photocurrent density was -10 mA cm⁻², the overpotential of NiCoP/g-C₃N₄ was -1.66 V vs. Ag/AgCl, which was lower than that of the

pristine g-C₃N₄ (-1.88 V vs. Ag/AgCl). Meanwhile, a photocurrent density of 16.05 mA cm⁻² could be achieved on NiCoP/g-C₃N₄ when potential was -1.8 V vs. Ag/AgCl, which was 2.3 times higher than that of the pristine g-C₃N₄ (6.82 mA cm⁻²). The reduced overpotential and increased photocurrent density would be efficiently promote the photocatalytic activity for H₂ production. Moreover, it has been reported that the overpotential of Ni_xP_y was decreased with the decrease of ratio between Ni and P [71]. In the study of Sun et al. [56], Ni₂P/g-C₃N₄ exhibited the lowest overpotential, similar to Pt/g-C₃N₄, followed by Ni₁₂P₅/g-C₃N₄, Ni₃P/g-C₃N₄ and g-C₃N₄ in sequence. In a word, the TMPs cocatalysts can significantly lower the overpotential of photocatalysts for HER, thereby improving the performance of photocatalytic H₂ production.

2.5. Strengthen photostability

From the view of practical applications, the photostability of photocatalysts is critical in photocatalytic H₂ production. As displayed in Fig. 3, the loading of TMPs on a semiconductor can efficiently strengthen photostability of the semiconductor photocatalyst by transferring the photogenerated charge carriers in time [72, 73]. For example, CdS is easily oxidized by photogenerated holes accumulated on its surface, leading to its self-decomposition [74]. Zhen et al. [68] developed core-shell structured Ni₂P@CdS photocatalyst with high activity and stability for H₂ production under visible light irradiation. The Ni₂P shell could restrain the self-decomposition of CdS core by separating the photogenerated holes for O₂ evolution. The Ni₂P@CdS exhibited excellent activity after four cycles, while the pure CdS displayed low stability after four cycles, indicating that the Ni₂P could suppress photocorrosion and improve stability of CdS. Meanwhile, the low concentration of Cd²⁺ and S²⁻ on the Ni₂P@CdS reaction systems during the four cycles also testified the anti-photocorrosion role of Ni₂P on CdS in the photocatalytic H₂ production. In the study of Cheng et al. [75], the FeP/CdS photocatalyst exhibited outstanding photostability in H₂ production even after

100 h of visible light irradiation. The strengthened photostability of FeP/CdS photocatalyst was attributed to the band bending between FeP and CdS, which accelerated the separation and transfer of photogenerated electron-hole pairs. Besides, black phosphorus (BP) also shows low stability in photocatalytic H₂ production because its edges are easily oxidized by dissolved oxygen [76]. Yuan et al. [77] found that the Co₂P cocatalyst selectively grown on the edges of BP nanosheets could suppress the oxidation of BP nanosheets via a contact inhibitor, hence improving the stability of Co₂P/BP photocatalyst. The H₂ production rate presented no obvious change and still remained at 97% after 12 h of photocatalytic reaction. Moreover, the high-resolution P 2p and Co 2p spectra before and after the reaction did not change significantly, further demonstrating the photostability of Co₂P/BP photocatalyst during the photocatalytic H₂ production. In brief, the TMPs cocatalysts can efficiently strengthen the photostability of the photocatalysts in photocatalytic H₂ production by reducing the contact of semiconductor photocatalysts with photogenerated holes or dissolved oxygen.

3. Synthetic strategies

Based on the phase of reactants, there are mainly two strategies to prepare TMPs for photocatalytic H₂ production, including solid-phase synthetic method and solution-phase synthetic method.

3.1. Solid-phase synthetic method

Solid-phase synthetic method is a process of mixing phosphorus source and solid metal source followed with thermal treatment under specific atmosphere. In this method, NaH₂PO₂ is widely utilized as phosphorus source because it can release PH₃ when the temperature exceeds 250 °C. The generated PH₃ can further directly react with solid precursors such as metal oxides, metal hydroxides, and metal-organic frameworks (MOFs) to form TMPs, as displayed in Fig. 4a. For example, CoP nanoparticles was successfully prepared by calcining the mixture of Co₃O₄ and NaH₂PO₂ at 300 °C

under N₂ atmosphere [78]. Li et al. [79] calcined the mixture of NiCo-MOF and NaH₂PO₂ at 350 °C under Ar atmosphere to obtain NiCoP₂. This method is beneficial to maintain the morphology and size of the precursors, but it is necessary to pay attention to the treatment of the toxic tail gas containing PH₃ in this process.

Moreover, direct reduction of metal orthophosphates by H₂ at a higher temperature is also a kind of solid-phase synthetic method to prepare TMPs, mainly utilized in MoP and WP. For example, Liu et al. [80] acquired a MoP precursor by evaporating and drying a homogeneous solution containing (NH₄)₆Mo₇O₂₄ · 4H₂O, (NH₄)₂HPO₄, citric acid and deionized water, and then calcining at 500 °C. Subsequently, they milled the MoP precursor and heated it at 850 °C under H₂/N₂ atmosphere to get MoP (Fig. 4b). Unfortunately, the TMPs obtained by this method present a large size and irregular morphology, which may reduce the number of active sites. Besides, TMPs can also be synthesized by high energy ball milling method. In this process, mixture of NaH₂PO₂ or phosphorus powders and metal source will be subjected to high-energy collision from milling media. Then, the TMPs is formed through an annealing treatment in an inert atmosphere. For example, Hu et al. [81] prepared CoP by high energy ball milling the mixture of red phosphorus and cobalt powder and annealing at 200 °C. Although solid-phase synthetic method is a cost-effective strategy for large-scale synthesis of TMPs, it usually requires longer reaction times, higher reaction temperatures and protection of an inert atmosphere. Meanwhile, it is often difficult to precisely control the morphology, size and purity of the TMPs.

3.2. Solution-phase synthetic method

The other strategy is solution-phase synthetic method. Tri-*n*-octylphosphine (TOP) is often utilized as a phosphorous source to prepare TMPs in organic solvent as its C-P covalent bond can be broken at a higher temperature. As a result, metal precursors including metal carbonyl compounds

and metal acetylacetonates can be phosphorized in the presence of TOP. For example, as shown in Fig. 4c, Zeng et al. [82] prepared Ni₂P nanoparticles by decomposing Ni(acac)₂ in oleylamine (OAm) at 210 °C, and subsequently reacting with TOP at 325 °C. However, the reaction is highly flammable and corrosive due to the use of organic solvent and high decomposition temperature of TOP, which hinders its application. Another solution-phase synthetic method is to use the sol-gel chemistry process to produce TMPs from a chemically homogeneous precursor. Generally, it can be completed at shorter reaction times and lower reaction temperature. Furthermore, it can better control the morphology and size of the TMPs. By using SiO₂ xerogel as the host matrix, Lukehart et al. [83] reported the synthesis of a series of TMPs by a sol-gel method followed by an annealing treatment. MoP/SiO₂ has also been synthesized using the same method [84].

Recently, hydrothermal/solvothermal method has been employed to synthesize TMPs because of the high efficiency and ease of the experimental process. In this process, a homogeneous solution including phosphorous source, metal source and solvent is transferred to the Teflon-lined stainless steel autoclave and then reacted at a specified temperature. The phosphorous source was mainly white phosphorous, yellow phosphorous, red phosphorous, and black phosphorous. For example, Fig. 4d demonstrated that red phosphorous (RP) and NiCl₂·6H₂O could be used as the precursors in the hydrothermal process to synthesize Ni₂P nanoparticles [85]. Sun et al. [86] prepared Ni₂P by a solvothermal reaction at 140 °C using yellow phosphorus as the phosphorous source, Ni(NO₃)₂·6H₂O as the metal source and ethylenediamine as the solvent. Additionally, sonochemical is also an effective solution-phase synthetic method for preparing TMPs, which helps to accelerate the reaction process and tune the morphology of TMPs. For example, FeP could be synthesized from the sonication of a mixture of Fe(CO)₅ and triethylphosphine solution with a power of 950 W for 300 min followed by the calcination at 950 °C [87]. Microwave-assisted synthesis can obtain TMPs in a

shorter time with lower power consumption due to the direct and uniform heating. For example, the preparation of Ni_2P and Ni_{12}P_5 only required 2 min of microwave irradiation using tetrabutylphosphonium chloride as phosphorus source and reaction medium [88].

4. Loading methods of TMPs on semiconductors

4.1. Post loading method

The post loading method is one of the strategies to load the TMPs cocatalysts on semiconductors. In this process, the TMPs are first synthesized and then combined with semiconductors through an extra loading method, such as physical grinding and impregnation. For example, Jin et al. [89] prepared TMPs/g- C_3N_4 nanocomposites by the physical grinding followed with annealing. As exhibited in Fig. 5a, the g- C_3N_4 nanosheets and TMPs were first synthesized by calcination and ultrasonication as well as hydrothermal process, respectively. Then, the g- C_3N_4 nanosheets and TMPs were mixed and ground in an agate mortar. Finally, the mixture was annealed in N_2 atmosphere at 200 °C to obtain the TMPs/g- C_3N_4 nanocomposites. Qin et al. [90] also loaded NiCoP@NiCo-Pi cocatalyst on g- C_3N_4 by the physical grinding. To increase the dispersibility of NiCoP@NiCo-Pi nanoparticles on the g- C_3N_4 surface, they added deionized water in the mixture during the grinding process, as shown in Fig. 5b.

Furthermore, impregnation method is an effective way to enhance the dispersibility of TMPs on semiconductors. For example, Liu et al. [91] combined carbon-encapsulated nickel phosphide (CNi_2P) with covalent organic polymer (COP-TF) by an ultrasonic-assisted self-assembly method. As depicted in Fig. 5c, the CNi_2P and COP-TF were first prepared by solvothermal reaction and copolymerization, respectively. Then the COP-TF@ CNi_2P photocatalyst was obtained by the ultrasonic-assisted self-assembly method. Because of the separate preparation of the TMPs cocatalysts and semiconductors, TMPs with different morphology and structure can be loaded. Kumar

et al. [92] prepared Ni₂P nanoparticles from porous Ni-MOFs and then deposited it on CdS via an impregnation method, as shown in Fig. 5d. The post loading method is conducive to the control of the morphology and size of TMPs. Nevertheless, the interfacial contact between TMPs cocatalysts and semiconductors is weak due to the separation treatment of this post loading method.

4.2. *In situ* reduction method

The loading of TMPs cocatalysts on semiconductors can also be performed by the in situ reduction method. This in situ growth method is beneficial for the formation of intimate contact and stable junction between TMPs cocatalysts and semiconductors, thus significantly promoting the transfer of photogenerated charge carriers. Generally, the in situ reduction process can be conducted using the chemical vapor deposition (CVD) method, the hydrothermal/solvothermal method and the photochemical reduction method. The CVD method is applicable to the phosphorization of metal, metal oxides and metal hydroxides. For example, Wang et al. [93] fabricated the Cu₃P/g-C₃N₄ photocatalyst via a facile CVD method. As shown in Fig. 6a, the few-layer g-C₃N₄ was prepared through the calcination and solvothermal process at first. Then the CuO was in situ grown on the few-layer g-C₃N₄. Finally, the Cu₃P/g-C₃N₄ was obtained by phosphorization treatment of CuO/g-C₃N₄.

The hydrothermal/solvothermal method is a facile and effective strategy to load TMPs cocatalysts in situ on semiconductors. Yuan et al. [77] reported that Co₂P could be selectively in situ grown around the edges of BP nanosheets through a simple solvothermal method. As exhibited in Fig. 6b, the few-layer BP nanosheets was first exfoliated from bulk BP in N-methyl-pyrrolidone (NMP) solution with the assistance of ultrasonication. Subsequently, the few-layer BP nanosheets reacted with Co(acac)₂ in N, N-dimethyl formamide (DMF) solution at 180 °C to in situ grow Co₂P around the edges of BP nanosheets. Besides, the in situ photodeposition of TMPs cocatalysts on semiconductors has also drawn attention because it can be executed at ambient temperature and does

not require extra reductant. In this process, the semiconductors absorb light and generate electron-hole pairs under irradiation. Then, part of $(\text{H}_2\text{PO}_2)^{-1}$ in the solution are reduced by the photogenerated electrons and react with metal ions to form TMPs [94, 95]. For example, Li et al. [96] deposited Ni_xP nanoparticles on the CdS@CuS nanowires via a photochemical reduction method, as displayed in Fig. 6c.

5. Application in photocatalytic H_2 production

Among all the studied TMPs, iron phosphides, cobalt phosphides and nickel phosphides are the most frequently used cocatalysts in photocatalytic H_2 production. Besides, copper phosphides, molybdenum phosphides, tungsten phosphides and bimetallic phosphides are also reported to be active in photocatalytic H_2 production as cocatalysts. In the following section, the performances and mechanisms of these TMPs in photocatalytic H_2 production are detailedly introduced and discussed.

5.1. Iron phosphides

Owing to their high abundance, extensive distribution, and low price, iron-based materials have been attractive in recent years [97-100]. Moreover, iron-containing clusters are the catalytically active sites in highly efficient biological H₂ catalysts such as [FeFe] and [Fe]-only hydrogenases [101]. These advantages render iron phosphides as efficient and inexpensive cocatalysts. And until now, iron phosphides have been extensively investigated and utilized in photocatalytic H_2 evolution system as cocatalysts [102, 103]. Iron phosphides usually exist in the form of FeP and Fe_2P . For example, Callejas et al. [104] immobilized hollow FeP nanoparticles on TiO_2 for photocatalytic H_2 production under ultraviolet light irradiation. The average H_2 production rate and the apparent quantum yield (AQY) at 365 nm for FeP/ TiO_2 were $1900 \mu\text{mol h}^{-1} \text{g}^{-1}$ and 8.7% in methanol aqueous solution, while TiO_2 alone exhibited an ignorable rate of H_2 production, indicating that FeP was the highly active cocatalyst in photocatalytic H_2 production.

Unfortunately, the practical application of FeP/TiO₂ was limited because it could only respond under ultraviolet light, which merely accounts for about 4% of the solar light. Therefore, it is significant to construct novel photocatalysts for H₂ production under visible light irradiation. Cheng et al. [75] found that FeP could improve the photocatalytic performance of CdS under visible light irradiation for H₂ production in lactic acid aqueous solution. The optimized FeP/CdS nanocomposites possessed a high H₂ production rate of 202000 $\mu\text{mol h}^{-1} \text{g}^{-1}$, which was approximately 67 and 3 times that of pure CdS and Pt/CdS, respectively. The yield of H₂ was dramatically enhanced because FeP could efficiently promote the separation of photogenerated charge from CdS. DFT calculations further clarified the photocatalytic mechanisms between FeP and CdS. When FeP and CdS were in close contact to form a heterojunction, an inherent electric field was built at their interface. This would shift the energy band edges of CdS downwards and the Fermi energy of FeP upwards to reach the equilibrium. The band bending could accelerate electron transfer from the CdS layer to the FeP layer at the interfacial space-charge region, and thus restrain the recombination of photogenerated electron-hole pairs. Meanwhile, the formation of the Schottky barrier also significantly promoted the spatial charge separation, resulting in the improved photocatalytic activity for H₂ production.

Although FeP could improve the photocatalytic H₂ production performance of CdS, the morphology of FeP/CdS nanocomposites in previous studies was mainly nanoparticles. The nanoparticles are easy to self-aggregate, which will result in a reduction in the number of active sites in photocatalytic reactions. Immobilizing cocatalysts nanoparticles on semiconductors nanosheets can efficiently resolve this issue, which not only increase the dispersion of cocatalysts but also promote the separation and transfer of photogenerated charge over semiconductors nanosheets. Sun et al. [105] fixed zero-dimensional (0D) FeP nanoparticles into two-dimensional (2D) CdS nanosheets for efficient photocatalytic H₂ production. The 0D FeP nanoparticles were uniformly dispersed on the

surface of 2D CdS nanosheets and a tight interfacial interaction was established on them. This intimate interfacial contact would facilitate the photogenerated charge transfer and separation, consequently increasing the yield of H₂. Specifically, under visible light irradiation, electrons in the valence band of 2D CdS nanosheets were excited to the CB, leaving holes in the valence band. Subsequently, photogenerated electrons accumulated on the CB migrated to the surface of 0D FeP nanoparticles through the close interfacial contact and reduced protons to H₂. Moreover, 2D g-C₃N₄ nanosheets was considered a good platform for dispersing 0D nanomaterials [106]. Zeng et al. [107] achieved superior photocatalytic H₂ production by uniformly depositing ultrasmall FeP nanodots on the 2D porous g-C₃N₄ nanosheets. Benefiting from the close contact between FeP and g-C₃N₄, the 0D/2D FeP/g-C₃N₄ presented accelerated photogenerated charge separation ability and enhanced photocatalytic H₂ production activity. The optimized FeP/g-C₃N₄ sample had a maximum H₂ production rate of 177.9 $\mu\text{mol h}^{-1} \text{g}^{-1}$ with the AQY of 1.57% at 420 nm.

In addition to FeP, Fe₂P was also employed as a cocatalyst for photocatalytic H₂ production owing to its good electronic conductivity [108, 109]. Sun et al. [110] reported that the photocatalytic H₂ production rate could be enhanced by more than 30 times by anchoring of Fe₂P nanoparticles on the surface of CdS nanorods. The enhanced activity was ascribed to the efficient transfer of photogenerated electrons from the CdS to the Fe₂P through the metal-semiconductor interfaces, facilitating the photogenerated charge separation. Meanwhile, the Fe₂P passivated the defects on the CdS surface, which made the electrons energetically favorable for photocatalytic H₂ production. Furthermore, Zhao et al. [54] prepared FeP and Fe₂P co-modified g-C₃N₄ photocatalyst for H₂ production under visible light irradiation. During the reaction, one proton in H₂O molecule was firstly adsorbed on the Fe(δ^+) and P(δ^-), respectively. Then the electrons in H-O bond migrated to the O atom to generate a dual protonation transition state and release OH⁻. Finally, as the photogenerated

electrons transfer from g-C₃N₄ to Fe(δ^+) atom, the hydride was formed around the Fe(δ^+) center, and further combined with the proton around the P(δ^-) to generate a H₂ molecule. As a result, because the Fe_xP cocatalyst could dramatically promote the separation and transfer of photogenerated electrons on g-C₃N₄ and the adjacent Fe and P atoms in Fe_xP could serve as dual proton adsorption sites, the H₂ production rate of optimized Fe_xP/g-C₃N₄ was 277 times higher than that of pristine g-C₃N₄.

5.2. Cobalt phosphides

Various cobalt phosphides as excellent cocatalysts for photocatalytic H₂ production have stimulated great interest (Table 2). Among these, CoP was investigated mostly, and a series of CoP-based photocatalysts were fabricated for photocatalytic H₂ production, such as CoP/Cd_xZn_{1-x}Se [111], CoP/BP [112], CoP/Zn_{0.5}Cd_{0.5}S [113], CoP/MIL-125-NH₂ [114], CoP/CeVO₄ [115], CdS@CoP@SiO₂ [116] and CdS/RGO-MoS₂@CoP [117]. For example, Yue et al. [118] found that CoP could significantly accelerate the photogenerated charge transfer and inhibit the photogenerated electron-hole pairs recombination of TiO₂, thereby enhancing the photocatalytic H₂ production rate. The H₂ production rate of the optimized CoP/TiO₂ was 8350 $\mu\text{mol h}^{-1} \text{g}^{-1}$, which was 11 times higher than that of the pristine TiO₂. Li et al. [119] reported that the introduction of CoP led to a remarkable enhancement in the photocatalytic H₂ production activity of g-C₃N₄. Compared to pure g-C₃N₄ (3.6 $\mu\text{mol h}^{-1} \text{g}^{-1}$), the resultant CoP/g-C₃N₄ presented superior photocatalytic H₂ production rate of 474.4 $\mu\text{mol h}^{-1} \text{g}^{-1}$. Tan et al. [120] loaded CoP on La, Cr: SrTiO₃ to obtain a novel photocatalyst with improved H₂ production activity. Due to the extended visible light response range and improved photogenerated charge transfer and separation, the photocatalytic H₂ production rate of the optimized CoP/La, Cr: SrTiO₃ was 27 times higher than that of La, Cr: SrTiO₃, reaching 198.4 $\mu\text{mol h}^{-1} \text{g}^{-1}$.

In addition to CoP, other phases of cobalt phosphides including Co₂P, CoP₃ and amorphous Co_xP have also drawn much attention. Li et al. [128] evenly dispersed Co₂P nanoparticles on the surface of

CdS sub-microspheres via an in situ hydrothermal method. The optimized Co₂P/CdS possessed a photocatalytic H₂ production rate of 6060 $\mu\text{mol h}^{-1} \text{g}^{-1}$, which was about 35 times higher than that of pure CdS. The enhanced photocatalytic activity resulted from the accelerated separation of photogenerated charge promoted by the proper band bending between Co₂P and CdS, as verified by the surface photovoltage (SPV) spectra and DFT calculation. Huang et al. [55] constructed a novel CoP₃/Mn_{0.2}Cd_{0.8}S nanocomposite, in which CoP₃ nanoparticles were homogeneously and tightly dispersed on the surface of Mn_{0.2}Cd_{0.8}S nanowires. The time-resolved photoluminescence (TRPL) spectra demonstrated that the introduction of CoP₃ prolonged the photogenerated charge lifetime of Mn_{0.2}Cd_{0.8}S (from 0.5256 to 0.8697 ns), thus promoting more photogenerated electrons participating in the photocatalytic H₂ production reaction. Accordingly, the superior H₂ production rate of 29530 $\mu\text{mol h}^{-1} \text{g}^{-1}$ was achieved on CoP₃/Mn_{0.2}Cd_{0.8}S under visible light irradiation, which was 5.02 times than that of pure Mn_{0.2}Cd_{0.8}S. Moreover, the amorphous CoP_x shell was loaded on CdS nanorods for photocatalytic H₂ production by Sun and co-workers [131]. The optimized CoP_x/CdS presented a H₂ production rate of 204000 $\mu\text{mol h}^{-1} \text{g}^{-1}$, which was much higher than that of pure CdS (25000 $\mu\text{mol h}^{-1} \text{g}^{-1}$). The AQY was measured to be 35% after 5 h of irradiation at 450 nm, suggesting the excellent photocatalytic H₂ production performance of CoP_x/CdS.

Despite enhanced photocatalytic H₂ production activity was achieved by introducing cobalt phosphides cocatalyst, there is still room for improvement. It has been reported that the nanostructure engineering could boost the HER performance of catalysts [132]. Therefore, cobalt phosphides with different morphologies were developed and utilized as cocatalysts in photocatalytic H₂ production, such as 0D quantum dots [133] and nanoparticles [126], one-dimensional (1D) nanowires [134] and nanorods [135], 2D nanosheets [136] and three-dimensional (3D) microspheres [137]. Luo et al. [124] incorporated 0D CoP nanoparticles into 2D g-C₃N₄ nanosheets through the electrostatic driven self-

assembly method and phosphorization method. Because the well dispersed 0D CoP nanoparticles (Fig. 7a) could provide more reaction active sites than the bulk CoP, the 0D/2D CoP/g-C₃N₄ nanohybrids exhibited a superior photocatalytic H₂ production rate of 1074 $\mu\text{mol h}^{-1} \text{g}^{-1}$, which was 41 times higher than that of the same mass bulk CoP modified g-C₃N₄. However, the 0D nanoparticles are difficult to be uniformly loaded on the surface of photocatalysts, and they tend to agglomerate and form large clusters.

One-dimensional nanostructured materials are believed to hold great application potential in the field of solar cells, electronic devices and photocatalysis due to their high aspect ratio and excellent electron transport property [138, 139]. Recently, 1D CoP nanowires with diameters about 100 nm were prepared via a low-temperature phosphidation of Co₃O₄ nanowires by Wang et al. [122], as displayed in Fig. 7b-d. The elemental mapping images in Fig. 7e further demonstrated that the elements of P and Co were uniformly distributed in the whole CoP nanowire. By introducing 1D CoP nanowires to Zn_{0.5}Cd_{0.5}S, the outstanding photocatalytic H₂ production activity was achieved (12175.8 $\mu\text{mol h}^{-1} \text{g}^{-1}$), which was 22 and 12 times higher than that of the pure Zn_{0.5}Cd_{0.5}S and the CoP nanoparticles modified Zn_{0.5}Cd_{0.5}S, respectively. The enhanced activity was attributed to the synergistic effect of the accelerated charge separation and transfer from Zn_{0.5}Cd_{0.5}S to CoP nanowires and the rapid H₂ production on 1D nanostructure.

Meanwhile, 2D nanomaterials have also received great attention for their exotic electronic properties and high specific surface areas. Wang et al. [62] designed a 2D/2D nanostructure constructed by CoP nanosheets and g-C₃N₄ nanosheets to expand the Schottky effect between their interfaces. As displayed in Fig. 7f-g, the CoP nanosheets were effectively combined with the g-C₃N₄ nanosheets, forming a well dispersed sheet-on-sheet structure. Both Co and P elements were homogeneously distributed throughout the 2D/2D CoP/g-C₃N₄ nanocomposite (Fig. 7h), suggesting

the inter-growth of the CoP nanosheets on the g-C₃N₄ nanosheets. Benefiting from the enhanced interaction, reduced self-agglomeration, enlarged Schottky effect, increased active sites, and shortened carrier transfer distances, the AQY of the 2D/2D CoP/g-C₃N₄ heterojunction was 2.1 times that of the corresponding 0D/2D heterojunction. In comparison with 0D, 1D and 2D nanostructures, 3D assemblies are more attractive owing to their unique architecture and properties. He et al. [137] demonstrated that 3D Co₂P microspheres were a good platform to load CdS nanowires (Fig. 7i-k), which uniformly dispersed on the surface of 3D Co₂P microspheres presented facilitated photogenerated charge separation and enhanced photocatalytic H₂ production activity.

Although a relatively high photogenerated charge carrier separation efficiency and high photocatalytic H₂ production activity were obtained in these photocatalysts, the understanding of the interfacial interactions and the formed chemical bonds between cobalt phosphides cocatalysts and semiconductor photocatalysts is still insufficient. In the past few years, only a few reports have explored the relationship between chemical bonds and photocatalytic performance. For example, Yuan et al. [77] found that the strong Co-P chemical bonds were formed between Co₂P and BP on the Co₂P/BP nanosheets photocatalyst. DFT calculations (Fig. 8a) demonstrated that the Co-P bonds could efficiently improve the photogenerated charge carrier transfer between the Co₂P layer and the BP layer in the atomic level. Therefore, the Co₂P/BP nanosheets photocatalyst presented an enhanced photocatalytic H₂ generation rate, which was 39.7 times higher than that of pure BP nanosheets. Moreover, the Co-S bonds in Co₂P/CdS photocatalyst were regarded as a Z-scheme “bridge” for charge transfer (Fig. 8b), which could significantly promote the separation of photogenerated electron-hole pairs and improve the photocatalytic H₂ production activity [127]. To deeply understand the chemical bonds and intrinsic active sites at atomic level, atomically dispersed catalysts have been developed in recent years. Liu et al. [130] confined a single Co₁-P₄ site on g-C₃N₄ nanosheets via a

facile phosphidation strategy (Fig. 8c). Correlated atomic characterizations corroborated that atomically dispersed Co atoms were successfully anchored by covalently forming an isolated Co₁-P₄ structure on g-C₃N₄ nanosheets. The atomically dispersed Co₁-phosphide active site could significantly inhibit charge recombination and prolong carrier lifetime by about 20 times relative to pristine g-C₃N₄, and promote H₂ production. Accordingly, the Co₁-phosphide/PCN photocatalyst owned exceptionally high photocatalytic activity, with H₂ production rates as high as 410.3 μmol h⁻¹ g⁻¹, which was 23 and 7.6 times higher than those of PCN and CoP cluster/PCN, respectively.

Apart from photocatalytic water splitting, photocatalytic formic acid (FA) dehydrogenation has also been considered as a promising method for H₂ production. Ultrasmall CoP nanoparticle was introduced as an efficient and robust cocatalyst for photocatalytic FA dehydrogenation by Cao and coworkers [140]. As shown in the DFT simulation in Fig. 9a-d in comparison with noble-metal Pt, CoP presented lower H₂ desorption energy in the H₂ production process, which would be beneficial for the H₂ production. When compounded with CdS@RGO, the hybrid possessed an excellent photocatalytic FA dehydrogenation rate of 182000 ± 12500 μmol h⁻¹ g⁻¹, which was more than 30 and 3 times higher than that of pure CdS and Pd/g-C₃N₄ photocatalysts, respectively. Moreover, Zhou et al. [141] implanted an atomically dispersed Co-P₃ species on CdS nanorods (CoPSA-CdS) for FA dehydrogenation under visible light irradiation. As revealed by the in situ attenuated total reflection infrared (ATR-IR) spectra (Fig. 9e-g), the CoPSA-CdS presented much better ability for FA dissociation adsorption and C-H bond activation than phosphorus-modified CdS (P-CdS) and sulfur-coordinated Co single atom-loaded CdS nanorods (CoSSA-CdS). DFT calculations (Fig. 9h-i) further verified that the Co-P₃ species accelerated the dissociation adsorption of FA by forming an active P-HCOO intermediate. Therefore, CoPSA-CdS photocatalyst exhibited an excellent photocatalytic activity for the dehydrogenation of FA to H₂.

5.3. Nickel phosphides

In the family of nickel phosphides, Ni_2P and Ni_{12}P_5 were the most studied materials as cocatalysts for photocatalytic H_2 production due to the excellent activity and stability (Table 3). For example, Wang et al. [142] anchored Ni_2P nanocrystals onto the g- C_3N_4 nanosheets through P-N chemical bonding. The presence of Ni_2P trapped the photogenerated electrons via a Z-scheme mechanism, thereby remarkably facilitating the separation of photogenerated electron-hole pairs and subsequent reduction of protons to produce H_2 . The optimized $\text{Ni}_2\text{P}/\text{g-}\text{C}_3\text{N}_4$ nanocomposite showed improved photocatalytic H_2 production rate of $362.4 \mu\text{mol h}^{-1} \text{g}^{-1}$ under visible light irradiation, which was about 22 times higher than that of pure g- C_3N_4 . Zeng et al. [143] embedded Ni_{12}P_5 nanoparticles into porous g- C_3N_4 nanosheets to enhance the photocatalytic H_2 production performance. The Ni_{12}P_5 nanoparticles could promote the transfer of photogenerated charges and serve as an active site for H_2 production. Benefiting from the accelerated charge transfer and increased catalytic site, the $\text{Ni}_{12}\text{P}_5/\text{g-}\text{C}_3\text{N}_4$ photocatalyst exhibited a superior photocatalytic activity for H_2 production. Moreover, Zhao et al. [144] reported that Ni_3P could be utilized as a cocatalyst for efficient photocatalytic H_2 production because of its excellent trapping-electron ability. To explore the phase effect of nickel phosphides on photocatalytic H_2 production, three different phases of nickel phosphides (Ni_2P , Ni_{12}P_5 , and Ni_3P) were prepared and then combined with g- C_3N_4 [56]. All three phases of nickel phosphides could efficiently enhance the photocatalytic activity of g- C_3N_4 for H_2 production, with the most significant effect of Ni_2P . This was because Ni_2P had a higher ratio of phosphorus, which could promote charge transfer and provide more Ni-P bonds, resulting in a superior H_2 production ability.

In order to further enhance the transfer ability of photogenerated charge carrier, a series of unique nanostructures have been designed to strengthen the interfacial contact between Ni_2P cocatalyst and semiconductor photocatalysts [156-158]. Zeng et al. [82] anchored monodisperse sub-15 nm Ni_2P

nanoparticles on porous g-C₃N₄ nanosheets to fabricate 0D/2D heterojunction interfaces (Fig. 10a). The 2D structure shortened the transfer distance of photogenerated charge carriers, and the Ni₂P accelerated the charge separation and transfer to inhibit the recombination of electron-hole pairs. Benefiting from the unique properties of 2D g-C₃N₄ nanosheets and 0D Ni₂P nanoparticles as well as the intimate contact between them, the 0D/2D Ni₂P/g-C₃N₄ nanocomposite presented significant enhanced photocatalytic H₂ production activity under visible light irradiation. Zhen et al. [68] constructed a core-shell structured Ni₂P@CdS photocatalyst for achieving highly efficient interfacial contact. As shown in Fig. 10b, the Ni₂P@CdS was a core-shell structure with a size of about 50 nm. Under visible light irradiation, the photogenerated electrons on the CB of CdS were migrated to the shell of Ni₂P. The shell of Ni₂P acted as both the platform to catch electrons and the reduction active site of proton to H₂. Therefore, the optimized Ni₂P@CdS photocatalyst exhibited a superior photocatalytic H₂ production rate of 838 $\mu\text{mol h}^{-1} \text{g}^{-1}$ revealing about 28.7-fold enhancement compared to that of the 1Pt@CdS. Furthermore, Boppella et al. [146] combined a 2D Ni₂P@BP cocatalyst with a 2D porous g-C₃N₄ nanosheets to improve the photocatalytic H₂ production. Fig. 10c demonstrated that a close interfacial contact was obtained between Ni₂P@BP nanosheets and g-C₃N₄ nanosheets. The BP nanosheets prevented the agglomeration of Ni₂P and build a strong ingenious interface with g-C₃N₄ nanosheets. Meanwhile, the uniformly distributed Ni₂P improved conductivity of the photocatalyst and provided abundant active sites for H₂ production. By virtue of these merits, the optimized 2D Ni₂P@BP/g-C₃N₄ photocatalyst displayed an excellent photocatalytic H₂ production activity of 858.2 $\mu\text{mol h}^{-1} \text{g}^{-1}$, which was about 50 times higher than that of the pure g-C₃N₄.

Besides, Ni₂P was also utilized in some complex photocatalytic H₂ production systems to meet the demand of practical application. Although 97% of the water resource on the earth is seawater,

effective photocatalytic H₂ production from seawater is still challenging due to the existence of complex and diverse cations and microorganisms. Liu et al. [91] loaded carbon-encapsulated Ni₂P on a fully conjugated organic polymer (COP-TF@CNi₂P) for stable and efficient photocatalytic H₂ production from seawater splitting. As exhibited in Fig. 10d, the optimized COP-TF@CNi₂P showed an excellent photocatalytic H₂ production rate of 2500 $\mu\text{mol h}^{-1} \text{g}^{-1}$, which was 10-fold higher than COP-TF@Pt from seawater. Moreover, the COP-TF@CNi₂P still kept 92% of photocatalytic efficiency after 16 intermittent cycles in seawater conditions, which lasted for half a month (Fig. 10e). The outstanding activity and long-term stability were owing to the compact integration between COP-TF and CNi₂P, which accelerated the transfer of photogenerated electrons to the surface of CNi₂P and resisted shedding during photocatalytic H₂ production. Recently, it has been found that microplastics are widely distributed in oceans, lakes, and drinking water, which will pose a great threat to human health. Photoreforming provides a novel strategy by not only reducing plastic pollution but also producing H₂ and valuable chemical products. For example, Uekert et al. [159] utilized CN_x/Ni₂P photocatalyst to produce H₂ and organic chemicals from poly(ethylene terephthalate) (PET) and poly(lactic acid) (PLA) under alkaline conditions. The strong binding of the Ni₂P cocatalyst to CN_x improved charge separation, thereby promoting photocatalytic activity. Moreover, CN_x/Ni₂P could also effectively and stably reform real-world polymer samples to produce H₂, as shown in Fig. 10f-h.

5.4. Others

Copper is one of the most abundant elements on the earth. Recently, p-type Cu₃P has been reported to be an ideal cocatalyst for photocatalytic H₂ production [160]. Sun et al. [161] loaded Cu₃P on CdS nanorods to form a p-n junction for accelerating charge transfer and enhancing photocatalytic H₂ production activity. The optimized Cu₃P/CdS presented excellent photocatalytic H₂ production rate of about 200000 $\mu\text{mol h}^{-1} \text{g}^{-1}$ under visible light irradiation, with the AQY of about 25% at 450

nm excitation. Yue et al. [162] found that the photocatalytic H₂ production rate of Cu₃P/TiO₂ was 11 times higher than that of pure TiO₂, which was attributed to the strong interaction between Cu₃P and TiO₂ induced accelerated separation of photogenerated electron-hole pairs. Moreover, Shen et al. [163] demonstrated that Cu₃P played an important role in improving the photocatalytic H₂ production activity of g-C₃N₄. To better understand the Cu₃P-induced charge antitrapping behavior in g-C₃N₄ (Fig. 11a), Wang et al. [93] employed femtosecond transient absorption (fs-TA) spectroscopy measurements to reveal the dynamics of charge carriers. As displayed in Fig. 11b-c, Cu₃P/g-C₃N₄ possessed a prolonged photogenerated excited electron lifetime (209 ps), indicating that Cu₃P could effectively promote transfer of photogenerated charge and inhibit recombination of photogenerated electron-hole pairs. Accordingly, the photocatalytic H₂ production rate of Cu₃P/g-C₃N₄ (277.2 μmol h⁻¹ g⁻¹) was 370 times higher than that of pure g-C₃N₄.

Among the earth abundant TMPs, molybdenum phosphides and tungsten phosphides have been determined as promising cocatalysts for photocatalytic H₂ production [164-168]. Yue et al. [169] attached MoP nanoparticles on the surface of CdS nanorods to form an intimate attachment (Fig. 11d and e) for H₂ production under visible light irradiation. The H₂ production rate of the optimized MoP/CdS (163200 μmol h⁻¹ g⁻¹) was more than 20 times higher than that of the pure CdS, which was ascribed to the suitable Fermi level alignment induced fast charge transfer in the interface of MoP and CdS. Meanwhile, Zhang et al. [170] found that WP could be used as an effective cocatalyst for improving the photocatalytic H₂ production activity of CdS. As exhibited in Fig. 11f and g, they deposited WP on the CdS support by a ball-milling method to generate a compact solid-solid interface. Benefiting from the suppressed recombination of the photogenerated electron-hole pairs, the WP/CdS obtained a superior H₂ production rate of 3104 μmol h⁻¹ g⁻¹, which was 11.67 times higher than that of the pure CdS.

In comparison with monometallic phosphides, bimetallic phosphides have a higher activity due to the synergistic effect of metallic elements [171-173]. Both of the active components in bimetallic phosphides can act as acceptors and transporters of electrons to facilitate the separation and transfer of charges, and further promote photocatalytic H₂ production [70, 174, 175]. For example, Xue et al. [176] decorated CoNiP onto PCN nanosheets for highly efficient photocatalytic H₂ production. Compared to Co₂P and Ni₂P, CoNiP was more conducive to the formation of H-H bond and the desorption of H₂ molecule. And it was found that the formation of P⁺-P^δ-Co/Ni^{δ+} chemical bridge between CoNiP and PCN could significantly boost charge transfer and separation. Thus, the photocatalytic H₂ production rate of CoNiP-PCN was up to 239.3 μmol h⁻¹ g⁻¹, which was higher than that of the Co₂P-PCN and Ni₂P-PCN. Zhu et al. [177] found that the absolute value of Gibbs free energies of NiFeP were reduced compared with Ni₂P and Fe₂P (Fig. 11h), which would be beneficial for the dissociation of H₂O and evolution of H₂. After introducing NiFeP into g-C₃N₄, the fluorescent lifetime was decayed from 8.77 ns to 5.21 ns, as shown in Fig. 11i. This result demonstrated that the photogenerated electrons of g-C₃N₄ were directly transferred to the surface of NiFeP, resulting in the worse delocalization ability of electrons and its easier reactions with protons to produce H₂. Therefore, the NiFeP/g-C₃N₄ possessed a higher H₂ production rate (3549 μmol h⁻¹ g⁻¹) than Ni₂P/g-C₃N₄ FeP/g-C₃N₄ (Fig. 11j).

6. Conclusions

In conclusion, this review summarizes the recent developments of TMPs cocatalyst in photocatalytic H₂ production. Firstly, the functions of TMPs in photocatalytic H₂ production are presented, mainly including enhancing light absorption, providing active sites, accelerating charge transfer, lowering overpotential and strengthening photostability. Then, the synthetic strategies of TMPs such as solid-phase synthetic method and solution-phase synthetic method are introduced.

Meanwhile, the loading methods of TMPs on semiconductor photocatalysts are summarized, such as post loading method and in situ reduction method. After that, the applications and mechanisms of the common TMPs (iron phosphides, cobalt phosphides, nickel phosphides, copper phosphides, molybdenum phosphides, tungsten phosphides and bimetallic phosphides) in photocatalytic H₂ production are discussed in detail.

7. Perspectives

Although some achievements in TMPs have been made, there are still many challenges to utilize TMPs cocatalysts for significant improvement in photocatalytic H₂ production. Some points are listed as follows.

- (1) Safer and quicker strategies for synthesizing TMPs should be developed. Most synthetic strategies to prepare TMPs require long reaction times, high reaction temperature and even protection of an inert atmosphere. Meanwhile, the toxic tail gas and the remaining organic solvent increase the environmental risks. Therefore, it is urgently to develop novel synthetic strategies for safely and quickly preparing TMPs.
- (2) Loading methods of TMPs on semiconductors should be optimized. Because of the low energy barrier at the interface of intimate junction, it is critical to optimize the loading methods for the fabrication of atomically well-bonded junction, which will significantly accelerate the charge transfer. In addition, such an intimate junction between the TMPs cocatalyst and semiconductors will strengthen photostability of the composite, which is beneficial for the practical application.
- (3) New types of TMPs cocatalysts and semiconductors should be explored. Among the various TMPs, iron phosphides, cobalt phosphides and nickel phosphides are the most frequently used cocatalysts in photocatalytic H₂ production. Although many other kinds of TMPs have proven to be efficient electrocatalysts for HER, the investigation on their application in photocatalytic H₂

application is still insufficient. Thus, it is very important to develop other types of TMPs for photocatalytic H₂ production. Meanwhile, in addition to combining the TMPs with the commonly used TiO₂, CdS and g-C₃N₄, other novel semiconductors should also be considered.

- (4) Highly active TMPs with different morphologies and structures should be developed. Currently, the morphology of most TMPs used for photocatalytic H₂ production is nanoparticles, which are easy to self-aggregate, resulting in a reduction in the number of active sites in photocatalytic reaction. Therefore, it is urgent to develop nanostructured TMPs with abundant active sites for assisting photocatalytic H₂ production, such as 2D ultrathin nanosheets, 0D quantum dots and single atoms.
- (5) Properties and functional mechanisms of the loaded photocatalysts should be deeply investigated. The effects of TMPs on the photocatalytic activity of the composites have been extensively studied. Nevertheless, the fundamental investigations on the physicochemical properties, photogenerated charge carrier dynamics and H₂ evolution mechanisms of loaded photocatalysts are scarce. Therefore, it is necessary to use some advanced technologies to solve these issues, such as in situ X-ray absorption spectroscopy and femtosecond transient absorption spectroscopy. Moreover, DFT calculations can be utilized to better design experiments and clarify mechanisms.
- (6) Impacts of sacrificial agents should be concerned. In photocatalytic H₂ production, sacrificial agents are usually added into the system to consume photogenerated holes for inhibiting the recombination of photogenerated electron-hole pairs. However, the addition of sacrificial agents may cause pollution to water, limiting sustainable practical applications. Combining H₂ evolution half-reaction with organic contaminants degradation or selective oxidation can resolve this issue. Accordingly, efforts should be made to replace sacrificial agents with the organic contaminants or the precursors of valuable chemical products in the future work.

(7) Overall water splitting should be considered. Current researches on TMPs cocatalysts are still focused on the H₂ evolution half-reaction. The ultimate objective in developing high efficiency TMPs co-catalysts is to realize the overall water splitting only by utilizing solar energy. Therefore, future studies of TMPs cocatalysts should be focused on the applications on overall water splitting.

Acknowledgements

This study was financially supported by the Program for the National Natural Science Foundation of China (51521006, 51879101, 51579098, 51779090, 51709101, 51809090), the Three Gorges Follow-up Research Project (2017HXXY-05), the National Program for Support of Top-Notch Young Professionals of China (2014), the Program for Changjiang Scholars and Innovative Research Team in University (IRT-13R17), Hunan Provincial Science and Technology Plan Project (2018SK20410, 2017SK2243, 2016RS3026), Hunan Provincial Innovation Foundation For Postgraduate (CX20190293), the Natural Science Foundation of Hunan Province, China (Grant Nos. 2019JJ50077), and the Fundamental Research Funds for the Central Universities (531119200086, 531118010114, 531107050978, 541109140001).

References

- [1] S. Tian, C. Zhang, D. Huang, R. Wang, G. Zeng, M. Yan, W. Xiong, C. Zhou, M. Cheng, W. Xue, Recent progress in sustainable technologies for adsorptive and reactive removal of sulfonamides, *Chem. Eng. J.*, 389 (2020) 123423.
- [2] Y. Fu, L. Qin, D. Huang, G. Zeng, C. Lai, B. Li, J. He, H. Yi, M. Zhang, M. Cheng, Chitosan functionalized activated coke for Au nanoparticles anchoring: Green synthesis and catalytic activities in hydrogenation of nitrophenols and azo dyes, *Appl. Catal. B: Environ.*, 255 (2019) 117740.
- [3] F. Qin, Y. Peng, G. Song, Q. Fang, R. Wang, C. Zhang, G. Zeng, D. Huang, C. Lai, Y. Zhou, Degradation of sulfamethazine by biochar-supported bimetallic oxide/persulfate system in natural water: Performance and reaction mechanism, *J. Hazard. Mater.*, 398 (2020) 122816.
- [4] S. Ye, G. Zeng, H. Wu, J. Liang, C. Zhang, J. Dai, W. Xiong, B. Song, S. Wu, J. Yu, The effects of activated biochar addition on remediation efficiency of co-composting with contaminated wetland soil, *Resour. Conserv. Recycl.*, 140 (2019) 278-285.
- [5] B. Li, C. Lai, M. Zhang, G. Zeng, S. Liu, D. Huang, L. Qin, X. Liu, H. Yi, F. Xu, Graphdiyne: A Rising Star of Electrocatalyst Support for Energy Conversion, *Adv. Energy Mater.*, 10 (2020) 2000177.
- [6] H. Luo, Z. Zeng, G. Zeng, C. Zhang, R. Xiao, D. Huang, C. Lai, M. Cheng, W. Yang, W. Xiong, Recent progress on metal-organic frameworks based-and derived-photocatalysts for water splitting, *Chem. Eng. J.*, 383 (2019) 123196.
- [7] Y. Liu, D. Huang, M. Cheng, Z. Liu, C. Lai, C. Zhang, C. Zhou, W. Xiong, F. Qin, B. Shao, Metal sulfide/MOF-based composites as visible-light-driven photocatalysts for enhanced hydrogen production from water splitting, *Coord. Chem. Rev.*, 409 (2020) 213220.
- [8] L. Lei, D. Huang, C. Zhang, R. Deng, S. Chen, Z. Li, F dopants triggered active sites in bifunctional cobalt sulfide@nickel foam toward electrocatalytic overall water splitting in neutral and alkaline media: Experiments and theoretical calculations, *J. Catal.*, 385 (2020) 129-139.
- [9] D. Huang, M. Wen, C. Zhou, Z. Li, M. Cheng, S. Chen, W. Xue, L. Lei, Y. Yang, W. Xiong, $Zn_xCd_{1-x}S$ based materials for photocatalytic hydrogen evolution, pollutants degradation and carbon dioxide reduction, *Appl. Catal. B: Environ.*, 267 (2020) 118651.
- [10] H. Feng, L. Tang, G. Zeng, J. Yu, Y. Deng, Y. Zhou, S. Wang, C. Feng, T. Luo, B. Shao, Electron density modulation of $Fe_{1-x}Co_xP$ nanosheet arrays by iron incorporation for highly efficient water splitting, *Nano Energy*, 67 (2020) 104174.
- [11] B. Song, M. Chen, G. Zeng, J. Gong, M. Shen, W. Xiong, C. Zhou, X. Tang, Y. Yang, W. Wang, Using graphdiyne (GDY) as a catalyst support for enhanced performance in organic pollutant degradation and hydrogen production: A review, *J. Hazard. Mater.*, 398 (2020) 122957.
- [12] A. Fujishima, K. Honda, Electrochemical photolysis of water at a semiconductor electrode, *Nature*, 238 (1972) 37-38.
- [13] Y. Yang, C. Zhang, C. Lai, G. Zeng, D. Huang, M. Cheng, J. Wang, F. Chen, C. Zhou, W. Xiong, $BiOX$ ($X = Cl, Br, I$) photocatalytic nanomaterials: applications for fuels and environmental management, *Adv. Colloid Interface Sci.*, 254 (2018) 76-93.
- [14] Y. Zhou, W. Wang, C. Zhang, D. Huang, C. Lai, M. Cheng, L. Qin, Y. Yang, C. Zhou, B. Li, Sustainable hydrogen production by molybdenum carbide-based efficient photocatalysts: From properties to mechanism, *Adv. Colloid Interface Sci.*, 279 (2020) 102144.
- [15] B.A. Pinaud, J.D. Benck, L.C. Seitz, A.J. Forman, Z. Chen, T.G. Deutsch, B.D. James, K.N. Baum, G.N. Baum, S. Ardo, Technical and economic feasibility of centralized facilities for solar hydrogen production via photocatalysis and photoelectrochemistry, *Energy Environ. Sci.*, 6 (2013) 1983-2002.
- [16] Y. Goto, T. Hisatomi, Q. Wang, T. Higashi, K. Ishikiriya, T. Maeda, Y. Sakata, S. Okunaka, H. Tokudome, M. Katayama, A particulate photocatalyst water-splitting panel for large-scale solar hydrogen generation, *Joule*, 2 (2018) 509-520.

- [17] D.M. Fabian, S. Hu, N. Singh, F.A. Houle, T. Hisatomi, K. Domen, F.E. Osterloh, S. Ardo, Particle suspension reactors and materials for solar-driven water splitting, *Energy Environ. Sci.*, 8 (2015) 2825-2850.
- [18] Z. Wang, C. Li, K. Domen, Recent developments in heterogeneous photocatalysts for solar-driven overall water splitting, *Chem. Soc. Rev.*, 48 (2019) 2109-2125.
- [19] S. Ye, M. Yan, X. Tan, J. Liang, G. Zeng, H. Wu, B. Song, C. Zhou, Y. Yang, H. Wang, Facile assembled biochar-based nanocomposite with improved graphitization for efficient photocatalytic activity driven by visible light, *Appl. Catal. B: Environ.*, 250 (2019) 78-88.
- [20] H. Guo, H. Niu, C. Liang, C. Niu, D. Huang, L. Zhang, N. Tang, Y. Yang, C. Feng, G. Zeng, Insight into the energy band alignment of magnetically separable $\text{Ag}_2\text{O}/\text{ZnFe}_2\text{O}_4$ pn heterostructure with rapid charge transfer assisted visible light photocatalysis, *J. Catal.*, 370 (2019) 289-303.
- [21] H. Guo, C. Niu, C. Feng, C. Liang, L. Zhang, X. Wen, Y. Yang, H. Liu, L. Li, L. Lin, Steering exciton dissociation and charge migration in green synthetic oxygen-substituted ultrathin porous graphitic carbon nitride for boosted photocatalytic reactive oxygen species generation, *Chem. Eng. J.*, 385 (2020) 123919.
- [22] X. Li, Z. Zeng, G. Zeng, D. Wang, R. Xiao, Y. Wang, C. Zhou, H. Yi, S. Ye, Y. Yang, A "bottle-around-ship" like method synthesized yolk-shell $\text{Ag}_3\text{PO}_4@\text{MIL-53}(\text{Fe})$ Z-scheme photocatalysts for enhanced tetracycline removal, *J. Colloid Interface Sci.*, 561 (2020) 501-511.
- [23] W. Xue, D. Huang, J. Li, G. Zeng, R. Deng, Y. Yang, S. Chen, Z. Li, X. Gong, B. Li, Assembly of AgI nanoparticles and ultrathin g- C_3N_4 nanosheets codecorated Bi_2WO_6 direct dual Z-scheme photocatalysts: An efficient, sustainable and heterogeneous catalyst with enhanced photocatalytic performance, *Chem. Eng. J.*, 375 (2019) 1144-1157.
- [24] Y. Yang, G. Zeng, D. Huang, C. Zhang, D. He, C. Zhou, W. Wang, W. Xiong, X. Li, B. Li, Molecular engineering of polymeric carbon nitride for highly efficient photocatalytic oxytetracycline degradation and H_2O_2 production, *Appl. Catal. B: Environ.*, 272 (2020) 118970.
- [25] Y. Yang, X. Li, X. Li, C. Zhou, W. Xiong, G. Zeng, D. Huang, C. Zhang, W. Wang, B. Song, X. Tang, X. Li, H. Guo, Recent advances in application of graphitic carbon nitride-based catalysts for degrading organic contaminants in water through advanced oxidation processes beyond photocatalysis: A critical review, *Water Res.*, 184 (2020) 116200.
- [26] Z. Wang, H. Wang, Z. Zeng, G. Zeng, P. Xu, R. Xiao, D. Huang, X. Chen, L. He, C. Zhou, Metal-organic Frameworks derived $\text{Bi}_2\text{O}_2\text{CO}_3$ /porous carbon nitride: A nanosized Z-scheme systems with enhanced photocatalytic activity, *Appl. Catal. B: Environ.*, 267 (2020) 118700.
- [27] Y. Wu, X. Li, Q. Yang, D. Wang, P. Yao, J. Cao, Z. Chen, X. Huang, Y. Yang, X. Li, Mxene-modulated dual-heterojunction generation on a metal-organic framework (MOF) via surface constitution reconstruction for enhanced photocatalytic activity, *Chem. Eng. J.*, 390 (2020) 124519.
- [28] Y. Liu, Z. Liu, D. Huang, M. Cheng, G. Zeng, C. Lai, C. Zhang, C. Zhou, W. Wang, D. Jiang, Metal or metal-containing nanoparticle@MOF nanocomposites as a promising type of photocatalyst, *Coord. Chem. Rev.*, 388 (2019) 63-78.
- [29] J. Willkomm, K.L. Orchard, A. Reynal, E. Pastor, J.R. Durrant, E. Reisner, Dye-sensitised semiconductors modified with molecular catalysts for light-driven H_2 production, *Chem. Soc. Rev.*, 45 (2016) 9-23.
- [30] W. Wang, P. Xu, M. Chen, G. Zeng, C. Zhang, C. Zhou, Y. Yang, D. Huang, C. Lai, M. Cheng, Alkali metal-assisted synthesis of graphite carbon nitride with tunable band-gap for enhanced visible-light-driven photocatalytic performance, *ACS Sustain. Chem. Eng.*, 6 (2018) 15503-15516.
- [31] Y. Yang, Z. Zeng, C. Zhang, D. Huang, G. Zeng, R. Xiao, C. Lai, C. Zhou, H. Guo, W. Xue, Construction of iodine vacancy-rich $\text{BiOI}/\text{Ag}@\text{AgI}$ Z-scheme heterojunction photocatalysts for visible-light-driven tetracycline degradation: transformation pathways and mechanism insight, *Chem. Eng. J.*, 349 (2018) 808-821.
- [32] C. Zhou, Z. Zeng, G. Zeng, D. Huang, R. Xiao, M. Cheng, C. Zhang, W. Xiong, C. Lai, Y. Yang, Visible-light-driven photocatalytic degradation of sulfamethazine by surface engineering of carbon nitride: Properties, degradation pathway and mechanisms, *J. Hazard. Mater.*, 380 (2019) 120815.

- [33] Y. Yang, Z. Zeng, G. Zeng, D. Huang, R. Xiao, C. Zhang, C. Zhou, W. Xiong, W. Wang, M. Cheng, Ti_3C_2 Mxene/porous g- C_3N_4 interfacial Schottky junction for boosting spatial charge separation in photocatalytic H_2O_2 production, *Appl. Catal. B: Environ.*, 258 (2019) 117956.
- [34] B. Song, Z. Zeng, G. Zeng, J. Gong, R. Xiao, S. Ye, M. Chen, C. Lai, P. Xu, X. Tang, Powerful combination of g- C_3N_4 and LDHs for enhanced photocatalytic performance: A review of strategy, synthesis, and applications, *Adv. Colloid Interface Sci.*, 271 (2019) 101999.
- [35] C. Zhou, G. Zeng, D. Huang, Y. Luo, M. Cheng, Y. Liu, W. Xiong, Y. Yang, B. Song, W. Wang, Distorted polymeric carbon nitride via carriers transfer bridges with superior photocatalytic activity for organic pollutants oxidation and hydrogen production under visible light, *J. Hazard. Mater.*, 386 (2020) 121947.
- [36] M. Jia, Z. Yang, H. Xu, P. Song, W. Xiong, J. Cao, Y. Zhang, Y. Xiang, J. Hu, C. Zhou, Integrating N and F co-doped TiO_2 nanotubes with ZIF-8 as photoelectrode for enhanced photo-electrocatalytic degradation of sulfamethazine, *Chem. Eng. J.*, 388 (2020) 124388.
- [37] Z. Li, D. Huang, C. Zhou, W. Xue, L. Lei, R. Deng, Y. Yang, S. Chen, W. Wang, Z. Wang, Metal-free carbon nitride with boosting photo-redox ability realized by the controlled carbon dopants, *Chem. Eng. J.*, 382 (2020) 122657.
- [38] J. Yang, D. Wang, H. Han, C. Li, Roles of cocatalysts in photocatalysis and photoelectrocatalysis, *Accounts Chem. Res.*, 46 (2013) 1900-1909.
- [39] W. Peng, Y. Li, F. Zhang, G. Zhang, X. Fan, Roles of two-dimensional transition metal dichalcogenides as cocatalysts in photocatalytic hydrogen evolution and environmental remediation, *Ind. Eng. Chem. Res.*, 56 (2017) 4611-4626.
- [40] Q. Xiang, J. Yu, M. Jaroniec, Synergetic effect of MoS_2 and graphene as cocatalysts for enhanced photocatalytic H_2 production activity of TiO_2 nanoparticles, *J. Am. Chem. Soc.*, 134 (2012) 6575-6578.
- [41] K. Chang, X. Hai, J. Ye, Transition Metal Disulfides as Noble-Metal Alternative Co-Catalysts for Solar Hydrogen Production, *Adv. Energy Mater.*, 6 (2016) 1502555.
- [42] A. Meng, L. Zhang, B. Cheng, J. Yu, Dual cocatalysts in TiO_2 photocatalysis, *Adv. Mater.*, 31 (2019) 1807660.
- [43] J. Ran, J. Zhang, J. Yu, M. Jaroniec, S.Z. Qiao, Earth-abundant cocatalysts for semiconductor-based photocatalytic water splitting, *Chem. Soc. Rev.*, 43 (2014) 7787-7812.
- [44] J. Ran, M. Jaroniec, S.Z. Qiao, Cocatalysts in semiconductor-based photocatalytic CO_2 reduction: achievements, challenges, and opportunities, *Adv. Mater.*, 30 (2018) 1701649.
- [45] P. Liu, J.A. Rodriguez, Catalysts for hydrogen evolution from the [NiFe] hydrogenase to the Ni_2P (001) surface: the importance of ensemble effect, *J. Am. Chem. Soc.*, 127 (2005) 14871-14878.
- [46] Y. Xu, R. Wu, J. Zhang, Y. Shi, B. Zhang, Anion-exchange synthesis of nanoporous FeP nanosheets as electrocatalysts for hydrogen evolution reaction, *Chem. Commun.*, 49 (2013) 6656-6658.
- [47] S. Cao, Y. Chen, C. Wang, P. He, W. Fu, Highly efficient photocatalytic hydrogen evolution by nickel phosphide nanoparticles from aqueous solution, *Chem. Commun.*, 50 (2014) 10427-10429.
- [48] S. Cao, Y. Chen, C. Hou, X. Lv, W. Fu, Cobalt phosphide as a highly active non-precious metal cocatalyst for photocatalytic hydrogen production under visible light irradiation, *J. Mater. Chem. A*, 3 (2015) 6096-6101.
- [49] S. Cao, Y. Chen, C. Wang, X. Lv, W. Fu, Spectacular photocatalytic hydrogen evolution using metal-phosphide/ CdS hybrid catalysts under sunlight irradiation, *Chem. Commun.*, 51 (2015) 8708-8711.
- [50] Y. Shi, B. Zhang, Recent advances in transition metal phosphide nanomaterials: synthesis and applications in hydrogen evolution reaction, *Chem. Soc. Rev.*, 45 (2016) 1529-1541.
- [51] M. Sun, H. Liu, J. Qu, J. Li, Earth-rich transition metal phosphide for energy conversion and storage, *Adv. Energy Mater.*, 6 (2016) 1600087.
- [52] S. Cao, C. Wang, W. Fu, Y. Chen, Metal phosphides as co-catalysts for photocatalytic and photoelectrocatalytic water splitting, *ChemSusChem*, 10 (2017) 4306-4323.
- [53] Y. Yang, G. Zeng, D. Huang, C. Zhang, D. He, C. Zhou, W. Wang, W. Xiong, B. Song, H. Yi, In Situ Grown Single-Atom Cobalt on Polymeric Carbon Nitride with Bidentate Ligand for Efficient Photocatalytic Degradation of Refractory

Antibiotics, Small, (2020) 2001634.

- [54] H. Zhao, J. Wang, Y. Dong, P. Jiang, Noble-metal-free iron phosphide cocatalyst loaded graphitic carbon nitride as an efficient and robust photocatalyst for hydrogen evolution under visible light irradiation, *ACS Sust. Chem. Eng.*, 5 (2017) 8053-8060.
- [55] Q. Huang, Z. Tao, L. Ye, H. Yao, Z. Li, $\text{Mn}_{0.2}\text{Cd}_{0.8}\text{S}$ nanowires modified by CoP_3 nanoparticles for highly efficient photocatalytic H_2 evolution under visible light irradiation, *Appl. Catal. B: Environ.*, 237 (2018) 689-698.
- [56] Z. Sun, M. Zhu, M. Fujitsuka, A. Wang, C. Shi, T. Majima, Phase effect of Ni_xP_y hybridized with g- C_3N_4 for photocatalytic hydrogen generation, *ACS Appl. Mater. Interfaces*, 9 (2017) 30583-30590.
- [57] H. An, X. Yan, H. Li, B. Yang, J. Wei, G. Yang, Increased Active Sites by in Situ Growth of CoP Quantum Dots on CdS/rGO To Achieve Efficient Photocatalytic H_2 Production, *ACS Applied Energy Materials*, 2 (2019) 4195-4204.
- [58] F. Zhang, J. Zhang, J. Li, X. Jin, Y. Li, M. Wu, X. Kang, T. Hu, X. Wang, W. Ren, Modulating charge transfer dynamics for g- C_3N_4 through a dimension and interface engineered transition metal phosphide co-catalyst for efficient visible-light photocatalytic hydrogen generation, *J. Mater. Chem. A*, 7 (2019) 6939-6945.
- [59] C. Li, Y. Du, D. Wang, S. Yin, W. Tu, Z. Chen, M. Kraft, G. Chen, R. Xu, Unique P-Co-N surface bonding states constructed on g- C_3N_4 nanosheets for drastically enhanced photocatalytic activity of H_2 evolution, *Adv. Funct. Mater.*, 27 (2017) 1604328.
- [60] J.F. Callejas, C.G. Read, C.W. Roske, N.S. Lewis, R.E. Schaak, Synthesis, Characterization, and Properties of Metal Phosphide Catalysts for the Hydrogen-Evolution Reaction, *Chem. Mater.*, 28 (2016) 6017-6044.
- [61] Y. Wang, B. Kong, D. Zhao, H. Wang, C. Selomulya, Strategies for developing transition metal phosphides as heterogeneous electrocatalysts for water splitting, *Nano Today*, 15 (2017) 26-55.
- [62] X. Wang, X. Tian, Y. Sun, J. Zhu, F. Li, H. Mu, J. Zhao, Enhanced Schottky effect of a 2D-2D $\text{CoP/g-C}_3\text{N}_4$ interface for boosting photocatalytic H_2 evolution, *Nanoscale*, 10 (2018) 12315-12321.
- [63] H. He, J. Cao, M. Guo, H. Lin, J. Zhang, Y. Chen, S. Chen, Distinctive ternary $\text{CdS/Ni}_2\text{P/g-C}_3\text{N}_4$ composite for overall water splitting: Ni_2P accelerating separation of photo carriers, *Appl. Catal. B: Environ.*, 249 (2019) 246-256.
- [64] B. Lin, J. Li, B. Xu, X. Yan, B. Yang, J. Wei, G. Yang, Spatial positioning effect of dual cocatalysts accelerating charge transfer in three dimensionally ordered macroporous g- C_3N_4 for photocatalytic hydrogen evolution, *Appl. Catal. B: Environ.*, 243 (2019) 94-105.
- [65] L. Feng, H. Xue, Advances in transition-metal phosphide applications in electrochemical energy storage and catalysis, *ChemElectroChem*, 4 (2017) 20-34.
- [66] J. Su, J. Zhou, L. Wang, C. Liu, Y. Chen, Synthesis and application of transition metal phosphides as electrocatalyst for water splitting, *Sci. Bull.*, 52 (2017) 653-644.
- [67] J. Zhu, G. Cheng, J. Xiong, W. Li, S. Dou, Recent Advances in Cu-Based Cocatalysts toward Solar-to-Hydrogen Evolution: Categories and Roles, *Solar RRL*, 3 (2019) 1900256.
- [68] W. Zhen, X. Ning, B. Yang, Y. Wu, Z. Li, G. Lu, The enhancement of CdS photocatalytic activity for water splitting via anti-photocorrosion by coating Ni_2P shell and removing nascent formed oxygen with artificial gill, *Appl. Catal. B: Environ.*, 221 (2018) 243-257.
- [69] Z. Sun, M. Zhu, X. Lv, Y. Liu, C. Shi, Y. Dai, A. Wang, T. Majima, Insight into iron group transition metal phosphides (Fe_2P , Co_2P , Ni_2P) for improving photocatalytic hydrogen generation, *Appl. Catal. B: Environ.*, 246 (2019) 330-336.
- [70] L. Bi, X. Gao, L. Zhang, D. Wang, X. Zou, T. Xie, Enhanced photocatalytic hydrogen evolution of $\text{NiCoP/g-C}_3\text{N}_4$ with improved separation efficiency and charge transfer efficiency, *ChemSusChem*, 11 (2018) 276-284.
- [71] Y. Pan, Y. Liu, J. Zhao, K. Yang, J. Liang, D. Liu, W. Hu, D. Liu, Y. Liu, C. Liu, Monodispersed nickel phosphide nanocrystals with different phases: synthesis, characterization and electrocatalytic properties for hydrogen evolution, *J. Mater. Chem. A*, 3 (2015) 1656-1665.
- [72] B. Weng, M. Qi, C. Han, Z. Tang, Y. Xu, Photocorrosion Inhibition of Semiconductor-Based Photocatalysts: Basic Principle, Current Development, and Future Perspective, *ACS Catal.*, 9 (2019) 4642-4687.

- [73] S. Chen, D. Huang, P. Xu, W. Xue, L. Lei, M. Cheng, R. Wang, X. Liu, R. Deng, Semiconductor-based photocatalysts for photocatalytic and photoelectrochemical water splitting: will we stop with photocorrosion?, *J. Mater. Chem. A*, 8 (2020) 2286-2322.
- [74] X. Ning, G. Lu, Photocorrosion inhibition of CdS-based catalysts for photocatalytic overall water splitting, *Nanoscale*, 12 (2020) 1213-1223.
- [75] H. Cheng, X. Lv, S. Cao, Z. Zhao, Y. Chen, W. Fu, Robustly photogenerating H₂ in water using FeP/CdS catalyst under solar irradiation, *Sci Rep*, 6 (2016) 19846.
- [76] A. Favron, E. Gaufres, F. Fossard, A. Phaneuflheureux, N.Y. Tang, P.L. Levesque, A. Loiseau, R. Leonelli, S. Francoeur, R. Martel, Photooxidation and quantum confinement effects in exfoliated black phosphorus, *Nat. Mater.*, 14 (2015) 826-832.
- [77] Y. Yuan, Z. Shen, S. Song, J. Guan, L. Bao, L. Pei, Y. Su, S. Wu, W. Bai, Z. Yu, Co-P bonds as atomic-level charge transfer channel to boost photocatalytic H₂ production of Co₂P/black phosphorus nanosheets photocatalyst, *ACS Catal.*, 9 (2019) 7801-7807.
- [78] Y. Zhong, Y. Wu, B. Chang, Z. Ai, K. Zhang, Y. Shao, L. Zhang, X. Hao, A CoP/CdS/WS₂ p-n-n tandem heterostructure: a novel photocatalyst for hydrogen evolution without using sacrificial agents, *J. Mater. Chem. A*, 7 (2019) 14638-14645.
- [79] K. Li, Y. Zhang, Y. Lin, K. Wang, F. Liu, Versatile functional porous cobalt-nickel phosphide-carbon cocatalyst derived from a metal-organic framework for boosting the photocatalytic activity of graphitic carbon nitride, *ACS Appl. Mater. Interfaces*, 11 (2019) 28918-28927.
- [80] W. Liu, J. Shen, Q. Liu, X. Yang, H. Tang, Porous MoP network structure as co-catalyst for H₂ evolution over g-C₃N₄ nanosheets, *Appl. Surf. Sci.*, 462 (2018) 822-830.
- [81] Y. Hu, M. Liu, Q. Yang, L. Kong, L. Kang, Facile synthesis of high electrical conductive CoP via solid-state synthetic routes for supercapacitors, *Journal of Energy Chemistry*, 26 (2017) 49-55.
- [82] D. Zeng, W. Xu, W.J. Ong, J. Xu, H. Ren, Y. Chen, H. Zeng, D. Peng, Toward noble-metal-free visible-light-driven photocatalytic hydrogen evolution: monodisperse sub-10 nm Ni₂P nanoparticles anchored on porous g-C₃N₄ nanosheets to engineer 0D-2D heterojunction interfaces, *Appl. Catal. B Environ.*, 221 (2018) 47-55.
- [83] C.M. Lukehart, S.B. Milne, S.R. Stock, Formation of Crystalline Nanoclusters of Fe₂P, RuP, Co₂P, Rh₂P, Ni₂P, Pd₅P₂, or PtP₂ in a Silica Xerogel Matrix from Single-Source Molecular Precursors, *Chem. Mater.*, 10 (1998) 903-908.
- [84] S. Gong, L. Liu, H. He, Q. Cui, Dibenzo[*a,h*]phenylene hydrodesulfurization over MoP/SiO₂ catalyst prepared with sol-gel method, *Korean J. Chem. Eng.*, 37 (2020) 1419-1422.
- [85] E. Liu, L. Qi, J. Chen, J. Fan, X. Hu, In situ fabrication of a 2D Ni₂P/red phosphorus heterojunction for efficient photocatalytic H₂ evolution, *Mater. Res. Bull.*, 115 (2019) 27-36.
- [86] Z. Sun, H. Zheng, J. Li, P. Du, Extraordinarily efficient photocatalytic hydrogen evolution in water using semiconductor nanorods integrated with crystalline Ni₂P cocatalysts, *Energy Environ. Sci.*, 8 (2015) 2668-2676.
- [87] J.D. Sweet, D.J. Casadonte, Sonochemical synthesis of iron phosphide, *Ultrason. Sonochem.*, 8 (2001) 97-101.
- [88] C. Zhang, B. Xin, Z. Xi, B. Zhang, Z. Li, H. Zhang, Z. Li, J. Hao, Phosphonium-Based Ionic Liquid: A New Phosphorus Source toward Microwave-Driven Synthesis of Nickel Phosphide for Efficient Hydrogen Evolution Reaction, *ACS Sustain. Chem. Eng.*, 6 (2018) 1468-1477.
- [89] C. Jin, C. Xu, W. Chang, X. Ma, X. Hu, E. Liu, J. Fan, Bimetallic phosphide NiCoP anchored g-C₃N₄ nanosheets for efficient photocatalytic H₂ evolution, *J. Alloys Compd.*, 803 (2019) 205-215.
- [90] Z. Qin, Y. Chen, Z. Huang, J. Su, L. Guo, A bifunctional NiCoP-based core/shell cocatalyst to promote separate photocatalytic hydrogen and oxygen generation over graphitic carbon nitride, *J. Mater. Chem. A*, 5 (2017) 19025-19035.
- [91] Y. Liu, Z. Xiang, Fully conjugated covalent organic polymer with carbon-encapsulated Ni₂P for highly sustained photocatalytic H₂ production from seawater, *ACS Appl. Mater. Interfaces*, 11 (2019) 41313-41320.
- [92] D.P. Kumar, J. Choi, S. Hong, D.A. Reddy, S. Lee, T.K. Kim, Rational synthesis of metal-organic framework-derived

- noble metal-free nickel phosphide nanoparticles as a highly efficient cocatalyst for photocatalytic hydrogen evolution, *ACS Sustain. Chem. Eng.*, 4 (2016) 7158-7166.
- [93] W. Wang, X. Zhao, Y. Cao, Z. Yan, R. Zhu, Y. Tao, X. Chen, D. Zhang, G. Li, D.L. Phillips, Copper phosphide-enhanced lower charge trapping occurrence in graphitic-C₃N₄ for efficient noble-metal-free photocatalytic H₂ evolution, *ACS Appl. Mater. Interfaces*, 11 (2019) 16527-16537.
- [94] Y. Dong, L. Kong, G. Wang, P. Jiang, N. Zhao, H. Zhang, Photochemical synthesis of Co_xP as cocatalyst for boosting photocatalytic H₂ production via spatial charge separation, *Appl. Catal. B: Environ.*, 211 (2017) 245-251.
- [95] Y. Dong, L. Kong, P. Jiang, G. Wang, N. Zhao, H. Zhang, B. Tang, A general strategy to fabricate Ni_xP as highly efficient cocatalyst via photoreduction deposition for hydrogen evolution, *ACS Sustain. Chem. Eng.*, 5 (2017) 6845-6853.
- [96] Y. Li, M. Qi, J. Li, Z. Tang, Y. Xu, Noble metal free CdS@CuS-Ni_xP hybrid with modulated charge transfer for enhanced photocatalytic performance, *Appl. Catal. B: Environ.*, 257 (2019) 117934.
- [97] W. Xiong, Z. Zeng, G. Zeng, Z. Yang, R. Xiao, X. Li, J. Cao, C. Zhou, H. Chen, M. Jia, Metal-organic frameworks derived magnetic carbon- α Fe/Fe₃C composites as a highly effective adsorbent for tetracycline removal from aqueous solution, *Chem. Eng. J.*, 374 (2019) 91-99.
- [98] H. Yi, M. Yan, D. Huang, G. Zeng, C. Lai, M. Li, X. Huo, L. Qin, S. Liu, X. Liu, Synergistic effect of artificial enzyme and 2D nano-structured Bi₂WO₆ for eco-friendly and efficient biomimetic photocatalysis, *Appl. Catal. B: Environ.*, 250 (2019) 52-62.
- [99] Y. Liu, M. Cheng, Z. Liu, G. Zeng, H. Zhong, M. Chen, C. Zhou, W. Xiong, B. Shao, B. Song, Heterogeneous Fenton-like catalyst for treatment of rhamnolipid-solubilized hexadecane wastewater, *Chemosphere*, 236 (2019) 124387.
- [100] W. Li, J. Cao, W. Xiong, Z. Yang, S. Sun, M. Jia, Z. Xu, In-situ growing of metal-organic frameworks on three-dimensional iron network as an efficient adsorbent for antibiotics removal, *Chem. Eng. J.*, 392 (2020) 124844.
- [101] S. Shima, O. Pilak, S. Vogt, M. Schick, M.S. Stagni, W. Meyer-Klaucke, E. Warkentin, R.K. Thauer, U. Ermler, The crystal structure of [Fe]-hydrogenase reveals the geometry of the active site, *Science*, 321 (2008) 572-575.
- [102] Y. Qi, J. Xu, Y. Fu, C. Wang, L. Wang, Metal-organic framework templated synthesis of g-C₃N₄/Fe₂O₃@FeP composites for enhanced hydrogen production, *ChemCatChem*, 11 (2019) 3465-3473.
- [103] C. Zhao, H. Tang, W. Liu, C. Han, X. Yang, Q. Liu, J. Xu, Constructing 0D FeP nanodots/2D g-C₃N₄ nanosheets heterojunction for highly improved photocatalytic hydrogen evolution, *ChemCatChem*, 11 (2019) 6310-6315.
- [104] J.F. Callejas, J.M. McEnaney, C.G. Head, J.C. Grompton, A.J. Biacchi, E.J. Popczun, T.R. Gordon, N.S. Lewis, R.E. Schaak, Electrocatalytic and photocatalytic hydrogen production from acidic and neutral-pH aqueous solutions using iron phosphide nanoparticles, *ACS nano*, 8 (2014) 11101-11107.
- [105] K. Sun, J. Shen, Y. Yang, H. Tang, C. Lei, Highly efficient photocatalytic hydrogen evolution from 0D/2D heterojunction of FeP nanoparticles/CdS nanosheets, *Appl. Surf. Sci.*, 505 (2020) 144042.
- [106] Y. Yang, C. Zhang, D. Huang, G. Zeng, J. Huang, C. Lai, C. Zhou, W. Wang, H. Guo, W. Xue, Boron nitride quantum dots decorated ultrathin porous g-C₃N₄: intensified exciton dissociation and charge transfer for promoting visible-light-driven molecular oxygen activation, *Appl. Catal. B: Environ.*, 245 (2019) 87-99.
- [107] D. Zeng, T. Zhou, W. Ong, M. Wu, X. Duan, W. Xu, Y. Chen, Y. Zhu, D. Peng, Sub-5 nm ultra-fine FeP nanodots as efficient co-catalysts modified porous g-C₃N₄ for precious-metal-free photocatalytic hydrogen evolution under visible light, *ACS Appl. Mater. Interfaces*, 11 (2019) 5651-5660.
- [108] Z. Pan, R. Wang, J. Li, S. Iqbal, W. Liu, K. Zhou, Fe₂P nanoparticles as highly efficient freestanding co-catalyst for photocatalytic hydrogen evolution, *Int. J. Hydrogen Energy*, 43 (2018) 5337-5345.
- [109] Z. Sun, M. Fujitsuka, C. Shi, M. Zhu, A. Wang, T. Majima, Efficient visible-light-driven hydrogen generation on g-C₃N₄ coupled with iron phosphide, *ChemPhotoChem*, 3 (2019) 540-544.
- [110] Z. Sun, H. Chen, Q. Huang, P. Du, Enhanced photocatalytic hydrogen production in water under visible light using noble metal-free ferrous phosphide as an active cocatalyst, *Catal. Sci. Technol.*, 5 (2015) 4964-4967.
- [111] B. Qiu, Q. Zhu, M. Xing, J. Zhang, A robust and efficient catalyst of Cd_xZn_{1-x}Se motivated by CoP for

photocatalytic hydrogen evolution under sunlight irradiation, *Chem. Commun.*, 53 (2017) 897-900.

[112] Q. Liang, F. Shi, X. Xiao, X. Wu, K. Huang, S. Feng, In situ growth of CoP nanoparticles anchored on black phosphorus nanosheets for enhanced photocatalytic hydrogen production, *ChemCatChem*, 10 (2018) 2179-2183.

[113] D. Dai, H. Xu, L. Ge, C. Han, Y. Gao, S. Li, Y. Lu, In-situ synthesis of CoP co-catalyst decorated Zn_{0.5}Cd_{0.5}S photocatalysts with enhanced photocatalytic hydrogen production activity under visible light irradiation, *Appl. Catal. B: Environ.*, 217 (2017) 429-436.

[114] Y. Li, Z. Jin, X. Hao, G. Wang, Insights into the unique role of cobalt phosphide for boosting hydrogen evolution activity based on MIL-125-NH₂, *Int. J. Hydrogen Energy*, 44 (2019) 17909-17921.

[115] L. Zhang, X. Hao, J. Li, Y. Wang, Z. Jin, Unique synergistic effects of ZIF-9 (Co)-derived cobalt phosphide and CeVO₄ heterojunction for efficient hydrogen evolution, *Chin. J. Catal.*, 41 (2020) 82-94.

[116] H. Li, X. Yan, B. Lin, M. Xia, J. Wei, B. Yang, G. Yang, Controllable spatial effect acting on photo-induced CdS@CoP@SiO₂ ball-in-ball nano-photoreactor for enhancing hydrogen evolution, *Nano Energy*, 47 (2018) 481-493.

[117] D.A. Reddy, J. Choi, S. Lee, Y. Kim, S. Hong, D.P. Kumar, T.K. Kim, Hierarchical dandelion-flower-like cobalt-phosphide modified CdS/reduced graphene oxide-MoS₂ nanocomposites as a noble-metal-free catalyst for efficient hydrogen evolution from water, *Catal. Sci. Technol.*, 6 (2016) 6197-6206.

[118] X. Yue, S. Yi, R. Wang, Z. Zhang, S. Qiu, Cobalt phosphide modified titanium oxide nanophotocatalysts with significantly enhanced photocatalytic hydrogen evolution from water splitting, *Small*, 13 (2017) 1603301.

[119] S. Yi, J. Yan, B. Wulan, S. Li, K. Liu, Q. Jiang, Noble-metal-free cobalt phosphide modified carbon nitride: an efficient photocatalyst for hydrogen generation, *Appl. Catal. B: Environ.*, 200 (2017) 477-483.

[120] P. Tan, A. Zhu, Y. Liu, Y. Ma, W. Liu, H. Cui, J. Pan, Insights into the efficient charge separation and transfer efficiency of La, Cr-codoped SrTiO₃ modified with CoP as a noble-metal-free co-catalyst for superior visible-light driven photocatalytic hydrogen generation, *Inorg. Chem. Front.*, 5 (2018) 579-586.

[121] Y. Liu, J. Zhang, X. Li, Z. Yao, L. Zhou, H. Sun, S. Wang, Graphitic carbon nitride decorated with CoP nanocrystals for enhanced photocatalytic and photoelectrochemical H₂ evolution, *Energy Fuels*, 33 (2019) 11663-11676.

[122] P. Wang, S. Zhan, H. Wang, Y. Xia, Q. Hou, Q. Zhang, Y. Li, R. Kumar, Cobalt phosphide nanowires as efficient co-catalyst for photocatalytic hydrogen evolution over Zn_{0.5}Cd_{0.5}S, *Appl. Catal. B: Environ.*, 230 (2018) 210-219.

[123] Q. Hua, X. Zhou, B. Zhang, M. Wang, J. Li, Y. Wang, L. Jiang, Band modulation and interfacial engineering to generate efficient visible-light-induced bifunctional photocatalysts, *ACS Sustain. Chem. Eng.*, 8 (2020) 2919-2930.

[124] B. Luo, R. Song, J. Geng, X. Li, D. Jing, M. Wang, C. Cheng, Towards the prominent cocatalytic effect of ultra-small CoP particles anchored on g-C₃N₄ nanosheets for visible light driven photocatalytic H₂ production, *Appl. Catal. B: Environ.*, 256 (2019) 117819.

[125] H. Li, J. Zhao, Y. Geng, Z. Li, Y. Li, J. Wang, Construction of CoP/B doped g-C₃N₄ nanodots/g-C₃N₄ nanosheets ternary catalysts for enhanced photocatalytic hydrogen production performance, *Appl. Surf. Sci.*, 496 (2019) 143738.

[126] J. Wang, P. Wang, C. Wang, Y. Ao, In-situ synthesis of well dispersed CoP nanoparticles modified CdS nanorods composite with boosted performance for photocatalytic hydrogen evolution, *Int. J. Hydrogen Energy*, 43 (2018) 14934-14943.

[127] N. Li, Y. Ding, J. Wu, Z. Zhao, X. Li, Y. Zheng, M. Huang, X. Tao, Efficient, full spectrum-driven H₂ Evolution Z-Scheme Co₂P/CdS photocatalysts with Co-S bonds, *ACS Appl. Mater. Interfaces*, 11 (2019) 22297-22306.

[128] S. Li, L. Wang, S. Liu, B. Xu, N. Xiao, Y. Gao, W. Song, L. Ge, J. Liu, In situ synthesis of strongly coupled Co₂P-CdS nanohybrids: an effective strategy to regulate photocatalytic hydrogen evolution activity, *ACS Sustain. Chem. Eng.*, 6 (2018) 9940-9950.

[129] Y. Chao, J. Zheng, H. Zhang, F. Li, F. Yan, Y. Tan, Z. Zhu, Oxygen-incorporation in Co₂P as a non-noble metal cocatalyst to enhance photocatalysis for reducing water to H₂ under visible light, *Chem. Eng. J.*, 346 (2018) 281-288.

[130] W. Liu, L. Cao, W. Cheng, Y. Cao, X. Liu, W. Zhang, X. Mou, L. Jin, X. Zheng, W. Che, Single-site active cobalt-based photocatalyst with a long carrier lifetime for spontaneous overall water splitting, *Angew. Chem. Int. Ed.*, 56 (2017)

9312-9317.

- [131] Z. Sun, B. Lv, J. Li, M. Xiao, X. Wang, P. Du, Core-shell amorphous cobalt phosphide/cadmium sulfide semiconductor nanorods for exceptional photocatalytic hydrogen production under visible light, *J. Mater. Chem. A*, 4 (2016) 1598-1602.
- [132] D. He, C. Zhang, G. Zeng, Y. Yang, D. Huang, L. Wang, H. Wang, A multifunctional platform by controlling of carbon nitride in the core-shell structure: from design to construction, and catalysis applications, *Appl. Catal. B: Environ.*, 117957 (2019) 117957.
- [133] K. Qi, W. Lv, I. Khan, S. Liu, Photocatalytic H₂ generation via CoP quantum-dot-modified g-C₃N₄ synthesized by electroless plating, *Chin. J. Catal.*, 41 (2020) 114-121.
- [134] J. Tian, N. Cheng, Q. Liu, W. Xing, X. Sun, Cobalt phosphide nanowires: efficient nanostructures for fluorescence sensing of biomolecules and photocatalytic evolution of dihydrogen from water under visible light, *Angew. Chem. Int. Ed.*, 54 (2015) 5493-5497.
- [135] D. Zeng, W. Ong, Y. Chen, S. Tee, C. Chua, D. Peng, M. Han, Co₂P nanorods as an efficient cocatalyst decorated porous g-C₃N₄ nanosheets for photocatalytic hydrogen production under visible light irradiation, *Part. Part. Syst. Charact.*, 35 (2018) 1700251.
- [136] Q. Gai, X. Zheng, W. Liu, Q. Dong, Y. Wang, R. Gao, S. Ren, 2D-2D heterostructured CdS-CoP photocatalysts for efficient H₂ evolution under visible light irradiation, *Int. J. Hydrogen Energy*, 44 (2019) 27411-27420.
- [137] Y. He, R. Cui, C. Gao, J. Zhang, X. Li, Cobalt phosphide microspheres integrated with cadmium sulfide nanowires as an efficient photocatalyst for hydrogen evolution reaction, *Molecular Catalysis*, 463 (2019) 161-166.
- [138] W. Wang, Z. Zeng, G. Zeng, C. Zhang, R. Xiao, C. Zhou, W. Xiong, Y. Yang, L. Lei, Y. Liu, Sulfur doped carbon quantum dots loaded hollow tubular g-C₃N₄ as novel photocatalyst for destruction of Escherichia coli and tetracycline degradation under visible light, *Chem. Eng. J.*, 378 (2019) 122133.
- [139] W. Wang, Q. Niu, G. Zeng, C. Zhang, D. Huang, B. Shao, C. Zhou, Y. Yang, Y. Liu, H. Guo, 1D porous tubular g-C₃N₄ capture black phosphorus quantum dots as 1D/0D metal-free photocatalysts for oxytetracycline hydrochloride degradation and hexavalent chromium reduction, *Appl. Catal. B: Environ.*, 273 (2020) 119051.
- [140] S. Cao, Y. Chen, H. Wang, J. Chen, X. Shi, H. Li, P. Cheng, X. Liu, M. Liu, L. Piao, Ultrasmall CoP nanoparticles as efficient cocatalysts for photocatalytic formic acid dehydrogenation, *Joule*, 2 (2018) 549-557.
- [141] P. Zhou, Q. Zhang, Z. Xu, Q. Shang, L. Wang, J. Chao, Y. Li, H. Chen, F. Lv, Q. Zhang, Atomically dispersed Co-P₃ on CdS nanorods with electron-rich surface boosts photocatalysis, *Adv. Mater.*, (2019) 1904249.
- [142] W. Wang, T. An, G. Li, D. Xia, H. Zhao, J.C. Yu, P.K. Wong, Earth-abundant Ni₂P/g-C₃N₄ lamellar nanohybrids for enhanced photocatalytic hydrogen evolution and bacterial inactivation under visible light irradiation, *Appl. Catal. B: Environ.*, 217 (2017) 570-580.
- [143] D. Zeng, W.J. Ong, H. Zheng, M. Wu, Y. Chen, D. Peng, M. Han, Ni₁₂P₅ nanoparticles embedded into porous g-C₃N₄ nanosheets as a noble-metal-free hetero-structure photocatalyst for efficient H₂ production under visible light, *J. Mater. Chem. A*, 5 (2017) 16171-16178.
- [144] J. Zhao, P. Liu, Y. Wang, Y. Li, M. Zu, C. Wang, X. Wang, L. Fang, H. Zeng, H. Yang, Metallic Ni₃P/Ni co-catalyst to enhance photocatalytic hydrogen evolution, *Chem. Eur. J.*, 23 (2017) 16734-16737.
- [145] J. Shi, Y. Zou, L. Cheng, D. Ma, D. Sun, S. Mao, L. Sun, C. He, Z. Wang, In-situ phosphating to synthesize Ni₂P decorated NiO/g-C₃N₄ p-n junction for enhanced photocatalytic hydrogen production, *Chem. Eng. J.*, 378 (2019) 122161.
- [146] R. Boppella, W. Yang, J. Tan, H. Kwon, J. Park, J. Moon, Black phosphorus supported Ni₂P co-catalyst on graphitic carbon nitride enabling simultaneous boosting charge separation and surface reaction, *Appl. Catal. B: Environ.*, 242 (2019) 422-430.
- [147] Z. Chen, Y. Yu, X. She, K. Xia, Z. Mo, H. Chen, Y. Song, J. Huang, H. Li, H. Xu, Constructing Schottky junction between 2D semiconductor and metallic nickel phosphide for highly efficient catalytic hydrogen evolution, *Appl. Surf. Sci.*, 495 (2019) 143528.

- [148] E. Liu, C. Jin, C. Xu, J. Fan, X. Hu, Facile strategy to fabricate Ni₂P/g-C₃N₄ heterojunction with excellent photocatalytic hydrogen evolution activity, *Int. J. Hydrogen Energy*, 43 (2018) 21355-21364.
- [149] J. Xu, J. Gao, Y. Qi, C. Wang, L. Wang, Anchoring Ni₂P on the UiO-66-NH₂/g-C₃N₄-derived C-doped ZrO₂/g-C₃N₄ heterostructure: highly efficient photocatalysts for H₂ production from water splitting, *ChemCatChem*, 10 (2018) 3327-3335.
- [150] T. Hu, K. Dai, J. Zhang, S. Chen, Noble-metal-free Ni₂P modified step-scheme SnNb₂O₆/CdS-diethylenetriamine for photocatalytic hydrogen production under broadband light irradiation, *Appl. Catal. B: Environ.*, 269 (2020) 118844.
- [151] T. Wu, P. Wang, J. Qian, Y. Ao, C. Wang, J. Hou, Noble-metal-free nickel phosphide modified CdS/C₃N₄ nanorods for dramatically enhanced photocatalytic hydrogen evolution under visible light irradiation, *Dalton Trans.*, 46 (2017) 13793-13801.
- [152] S. Kampouri, T.N. Nguyen, C.P. Ireland, B. Valizadeh, F.M. Ebrahim, G. Capano, D. Ongari, A. Mace, N. Guijarro, K. Sivula, Photocatalytic hydrogen generation from a visible-light responsive metal-organic framework system: the impact of nickel phosphide nanoparticles, *J. Mater. Chem. A*, 6 (2018) 2476-2481.
- [153] S. Peng, Y. Yang, J. Tan, C. Gan, Y. Li, In situ loading of Ni₂P on Cd_{0.5}Zn_{0.5}S with red phosphorus for enhanced visible light photocatalytic H₂ evolution, *Appl. Surf. Sci.*, 447 (2018) 822-828.
- [154] S. Dhingra, C. Nagaraja, Highly efficient visible-light-assisted photocatalytic hydrogen generation from water splitting catalyzed by Zn_{0.5}Cd_{0.5}S/Ni₂P heterostructures, *Int. J. Hydrogen Energy*, 43 (2018) 22917-22928.
- [155] D. Zeng, Z. Lu, X. Gao, B. Wu, W. Ong, Hierarchical flower-like Zn_{0.5}S₄ anchored with well-dispersed Ni₁₂P₅ nanoparticles for high-quantum-yield photocatalytic H₂ evolution under visible light, *Catal. Sci. Technol.*, 9 (2019) 4010-4016.
- [156] K. Wu, P. Wu, J. Zhu, C. Liu, X. Dong, J. Wu, G. Meng, K. Xu, J. Hou, Z. Liu, Synthesis of hollow core-shell CdS@TiO₂/Ni₂P photocatalyst for enhancing hydrogen evolution and degradation of MB, *Chem. Eng. J.*, 360 (2019) 221-230.
- [157] S. Zhao, J. Xu, Z. Li, Z. Liu, Y. Li, Molybdenum disulfide coated nickel-cobalt sulfide with nickel phosphide loading to build hollow core-shell structure for highly efficient photocatalytic hydrogen evolution, *J. Colloid Interface Sci.*, 555 (2019) 689-701.
- [158] P. Wen, K. Zhao, H. Li, J. Li, J. Li, Q. Ma, B.M. Mayer, L. Jiang, Y. Qiu, In situ decorated Ni₂P nanocrystal cocatalysts on g-C₃N₄ for efficient and stable photocatalytic hydrogen evolution via a facile co-heating method, *J. Mater. Chem. A*, 8 (2020) 2995.
- [159] T. Uekert, H. Kasap, E. Reimer, Photoreforming of nonrecyclable plastic waste over a carbon nitride/nickel phosphide catalyst, *J. Am. Chem. Soc.*, 141 (2019) 15201-15210.
- [160] R. Shen, J. Xie, Y. Ding, S. Liu, A. Adamski, X. Chen, X. Li, Carbon nanotube-supported Cu₃P as high-efficiency and low-cost cocatalysts for exceptional semiconductor-free photocatalytic H₂ evolution, *ACS Sustain. Chem. Eng.*, 7 (2018) 3243-3250.
- [161] Z. Sun, Q. Yue, J. Li, J. Xu, H. Zheng, P. Du, Copper phosphide modified cadmium sulfide nanorods as a novel p-n heterojunction for highly efficient visible-light-driven hydrogen production in water, *J. Mater. Chem. A*, 3 (2015) 10243-10247.
- [162] X. Yue, S. Yi, R. Wang, Z. Zhang, S. Qiu, A novel and highly efficient earth-abundant Cu₃P with TiO₂ "P-N" heterojunction nanophotocatalyst for hydrogen evolution from water, *Nanoscale*, 8 (2016) 17516-17523.
- [163] R. Shen, J. Xie, X. Lu, X. Chen, X. Li, Bifunctional Cu₃P decorated g-C₃N₄ nanosheets as a highly active and robust visible-light photocatalyst for H₂ production, *ACS Sustain. Chem. Eng.*, 6 (2018) 4026-4036.
- [164] S. Yin, J. Han, Y. Zou, T. Zhou, R. Xu, A highly efficient noble metal free photocatalytic hydrogen evolution system containing MoP and CdS quantum dots, *Nanoscale*, 8 (2016) 14438-14447.
- [165] Z. Jin, Y. Zhang, Q. Ma, Orthorhombic WP co-catalyst coupled with electron transfer bridge UiO-66 for efficient visible-light-driven H₂ evolution, *J. Colloid Interface Sci.*, 556 (2019) 689-703.

- [166] Y. Song, X. Xin, S. Guo, Y. Zhang, L. Yang, B. Wang, X. Li, One-step MOFs-assisted synthesis of intimate contact MoP-Cu₃P hybrids for photocatalytic water splitting, *Chem. Eng. J.*, 384 (2020) 123337.
- [167] C. Cheng, S. Zong, J. Shi, F. Xue, Y. Zhang, X. Guan, B. Zheng, J. Deng, L. Guo, Facile preparation of nanosized MoP as cocatalyst coupled with g-C₃N₄ by surface bonding state for enhanced photocatalytic hydrogen production, *Appl. Catal. B: Environ.*, 265 (2020) 118620.
- [168] Z. Yang, Z. Xing, Q. Feng, H. Jiang, J. Zhang, Y. Xiao, Z. Li, P. Chen, W. Zhou, Sandwich-like mesoporous graphite-like carbon nitride (Meso-g-C₃N₄)/WP/Meso-g-C₃N₄ laminated heterojunctions solar-driven photocatalysts, *J. Colloid Interface Sci.*, 568 (2020) 255-263.
- [169] Q. Yue, Y. Wan, Z. Sun, X. Wu, Y. Yuan, P. Du, MoP is a novel, noble-metal-free cocatalyst for enhanced photocatalytic hydrogen production from water under visible light, *J. Mater. Chem. A*, 3 (2015) 16941-16947.
- [170] J. Zhang, W. Yao, C. Huang, P. Shi, Q. Xu, High efficiency and stable tungsten phosphide cocatalysts for photocatalytic hydrogen production, *J. Mater. Chem. A*, 5 (2017) 12513-12519.
- [171] R. Shen, W. Liu, D. Ren, J. Xie, X. Li, Co_{1.4}Ni_{0.6}P cocatalysts modified metallic carbon black/g-C₃N₄ nanosheet Schottky heterojunctions for active and durable photocatalytic H₂ production, *Appl. Surf. Sci.*, 466 (2019) 393-400.
- [172] X. Lv, X. Li, C. Yang, X. Ding, Y. Zhang, Y. Zheng, S. Li, X. Sun, X. Tao, Large-size, porous, ultrathin NiCoP nanosheets for efficient electro/photocatalytic water splitting, *Adv. Funct. Mater.*, (2020) 1910830.
- [173] H. Feng, J. Yu, L. Tang, G. Zeng, W. Tang, J. Wang, T. Luo, B. Peng, B. Song, L. Wang, Tuning electron density endows Fe_{1-x}Co_xP with exceptional capability of electrooxidation of organic pollutants, *Environ. Sci. Technol.*, 53 (2019) 13878-13887.
- [174] S. Li, L. Wang, N. Xiao, A. Wang, X. Li, Y. Gao, N. Li, W. Song, L. Ge, J. Liu, In-situ synthesis of ternary metal phosphides Ni_xCo_{1-x}P decorated Zn_{0.5}Cd_{0.5}S nanorods with significantly enhanced photocatalytic hydrogen production activity, *Chem. Eng. J.*, 378 (2019) 122220.
- [175] S. Li, J. Tan, Z. Jiang, J. Wang, Z. Li, MOF-derived bimetallic Fe-Ni-P nanotubes with tunable compositions for dye-sensitized photocatalytic H₂ and O₂ production, *Chem. Eng. J.*, 384 (2020) 123354.
- [176] F. Xue, Y. Si, M. Wang, M. Liu, L. Guo, Toward efficient photocatalytic pure water splitting for simultaneous H₂ and H₂O₂ production, *Nano Energy*, 62 (2019) 823-831.
- [177] Q. Zhu, B. Qiu, H. Duan, Y. Gong, Z. Qin, B. Shen, M. Xing, J. Zhang, Electron directed migration cooperated with thermodynamic regulation over bimetallic NiFe₂/g-C₃N₄ for enhanced photocatalytic hydrogen evolution, *Appl. Catal. B: Environ.*, 259 (2019) 118078.

Table 1

Price of common cocatalysts.

Cocatalysts	CAS Number	Properties	Price (USD g ⁻¹)
Pt	7440-06-4	wire, diam. 2.0 mm, 99.9% trace metals basis	376.43
Pd	7440-05-3	powder, <1 μ m, \geq 99.9% trace metals basis	153.00
Au	7440-57-5	nanopowder, <100 nm particle size, 99.9% trace metals basis	405.00
Ag	7440-22-4	nanopowder, <150 nm particle size, 99% trace metals basis	31.20
Ru	7440-18-8	powder, 99.99% trace metals basis	211.00
Rh	7440-16-6	powder, 99.95% trace metals basis	611.00
Fe ₂ P	1310-43-6	99.5% trace metals basis	18.18
Ni ₂ P	12035-64-2	-100 mesh, 98%	11.40

CAS: Chemical Abstracts Service; USD: United States dollar. (Price data came from Sigma-Aldrich: 7/20/2020)

Accepted MS

Table 2Cobalt phosphides cocatalysts for photocatalytic H₂ production.

Photocatalyst	Cocatalyst	Light source	Sacrificial agents	Activity ($\mu\text{mol h}^{-1} \text{g}^{-1}$)	AQY (%) λ (nm)	Ref. (year)
CoP/g-C ₃ N ₄	CoP	UV-Vis (Xe)	Methanol	1038.1	1.10 (380)	[121] (2019)
CoP/TiO ₂	CoP	UV-Vis (Xe)	TEOA	8350	3.80 (350)	[118] (2017)
CoP/Zn _{0.5} Cd _{0.5} S	CoP	AM 1.5G (Xe)	Ascorbic acid	12175.8	4.37 (420)	[122] (2018)
CoP/CdS/WS ₂	CoP	$\lambda > 420$ nm (Xe)	-	9.16	1.34 (420)	[78] (2019)
CoP/P-g-C ₃ N ₄	CoP	$\lambda > 420$ nm (Xe)	Methanol	724	8.5 (420)	[123] (2020)
CoP/g-C ₃ N ₄	CoP	$\lambda > 420$ nm (Xe)	TEOA	956.8	3.65 (420)	[58] (2019)
CoP/g-C ₃ N ₄	CoP	$\lambda > 420$ nm (Xe)	TEOA	1074	6.10 (420)	[124] (2019)
CoP/BCNDs/CNNS	CoP	$\lambda > 420$ nm (Xe)	TEOA	1332.81	10.78 (420)	[125] (2019)
CoP/CdS	CoP	$\lambda > 420$ nm (Xe)	Na ₂ S + Na ₂ SO ₃	13785	11.60 (420)	[126] (2018)
CdS@CoP@SiO ₂	CoP	$\lambda > 420$ nm (Xe)	LA	17727	23.60 (435)	[116] (2018)
Co ₂ P/BP	Co ₂ P	$\lambda > 420$ nm (Xe)	Na ₂ S + Na ₂ SO ₃	202	2.42 (420)	[77] (2019)
Co ₂ P/CdS	Co ₂ P	$\lambda > 780$ nm (MH)	Lactic acid	3930	2.26 (700)	[127] (2019)
Co ₂ P/CdS	Co ₂ P	$\lambda > 420$ nm (Xe)	LA + K ₂ HPO ₄	712.90	3.88 (420)	[128] (2018)
o-Co ₂ P/CdS	Co ₂ P	$\lambda > 420$ nm (Xe)	LA	17448	22.17 (420)	[129] (2019)
CoP ₃ /Mn _{0.2} Cd _{0.8} S	CoP ₃	$\lambda > 420$ nm (Xe)	Na ₂ S + Na ₂ SO ₃	29550	29.20 (420)	[55] (2018)
Co ₁ -phosphide/PCN	CoP ₄	$\lambda > 420$ nm (Xe)	-	126.8	2.20 (500)	[130] (2017)

AQY: apparent quantum yield; Xe: xenon lamp; MH: metal halide lamp; TEOA: triethanolamine; LA: lactic acid.

Table 3Nickel phosphides cocatalysts for photocatalytic H₂ production.

Photocatalyst	Cocatalyst	Light source	Sacrificial agents	Activity ($\mu\text{mol h}^{-1} \text{g}^{-1}$)	AQY (%) λ (nm)	Ref. (year)
CdS/Ni ₂ P/g-C ₃ N ₄	Ni ₂ P	$\lambda > 420$ nm (Xe)	-	15.66	0.18 (420)	[63] (2019)
NiO/Ni ₂ P/CN	Ni ₂ P	$\lambda > 420$ nm (Xe)	TEOA	504	0.22 (400)	[145] (2019)
Ni ₂ P@BP/CN	Ni ₂ P	$\lambda > 420$ nm (Xe)	TEOA	858.2	2.80 (420)	[146] (2018)
Ni ₂ P/g-C ₃ N ₄	Ni ₂ P	$\lambda > 400$ nm (Xe)	TEOA	2337.09	3.98 (420)	[147] (2019)
Ni ₂ P/g-C ₃ N ₄	Ni ₂ P	UV-Vis (Xe)	TEOA	3344	9.10 (420)	[148] (2018)
C-ZrO ₂ /g-C ₃ N ₄ /Ni ₂ P	Ni ₂ P	$\lambda > 420$ nm (Xe)	TEOA	10040	35.5 (420)	[149] (2018)
Ni ₂ P/SNO/CdS-D	Ni ₂ P	$\lambda > 420$ nm (Xe)	Na ₂ S + Na ₂ SO ₃	11992	35.8 (420)	[150] (2020)
Ni ₂ P/CdS/g-C ₃ N ₄	Ni ₂ P	$\lambda > 400$ nm (Xe)	Na ₂ S + Na ₂ SO ₃	44450	46.3 (420)	[151] (2017)
Ni ₂ P/MIL-125-NH ₂	Ni ₂ P	$\lambda > 420$ nm (Xe)	TEOA	894	27 (400)	[152] (2018)
COP-TF@CNi ₂ P	Ni ₂ P	$\lambda > 400$ nm (Xe)	Na ₂ S + Na ₂ SO ₃	2500	2.50 (400)	[91] (2019)
Ni ₂ P/Cd _{0.5} Zn _{0.5} S	Ni ₂ P	$\lambda > 420$ nm (Xe)	Na ₂ S + Na ₂ SO ₃	1312	29 (420)	[153] (2018)
Ni ₂ P/Zn _{0.5} Cd _{0.5} S	Ni ₂ P	$\lambda > 420$ nm (LED)	Na ₂ S + Na ₂ SO ₃	2119	21.16 (450)	[154] (2018)
Ni ₁₂ P ₅ /g-C ₃ N ₄	Ni ₁₂ P ₅	$\lambda > 420$ nm (Xe)	TEOA	53.7	4.67 (420)	[143] (2017)
Ni ₁₂ P ₅ /ZnIn ₂ S ₄	Ni ₁₂ P ₅	$\lambda > 420$ nm (Xe)	Na ₂ S + Na ₂ SO ₃	226.3	20.50 (420)	[155] (2019)
CdS@CuS-Ni ₃ P	Ni ₃ P	$\lambda > 420$ nm (Xe)	Na ₂ S + Na ₂ SO ₃	18.60	13.06 (420)	[96] (2019)

AQY: apparent quantum yield; Xe: xenon lamp; TEOA: triethanolamine.

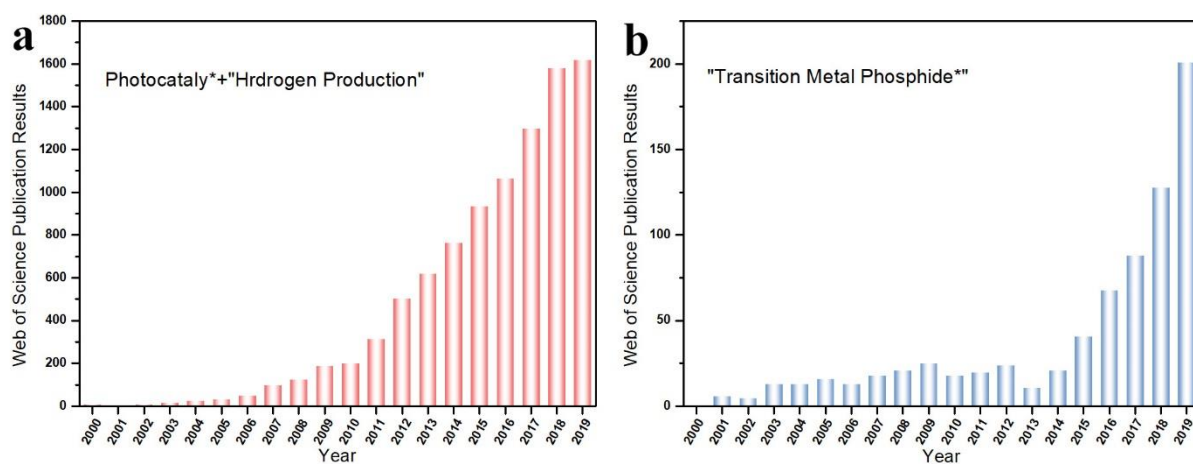


Fig. 1. Histogram of number of publications on (a) photocatalytic H₂ production and (b) transition metal phosphides from 2000 to 2019 (date source: Web of Science).

Accepted MS

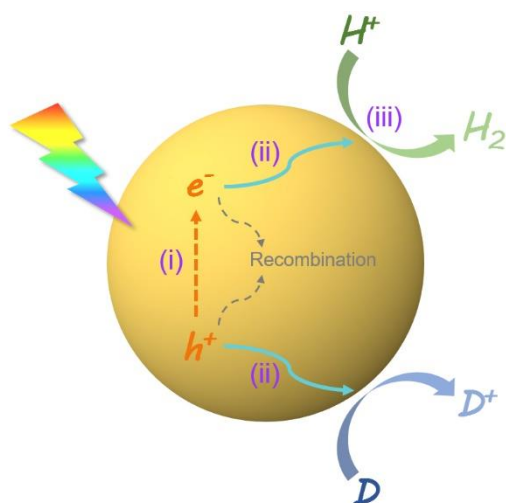


Fig. 2. Schematic illustration of photocatalytic H_2 production over a semiconductor photocatalyst.

Accepted MS

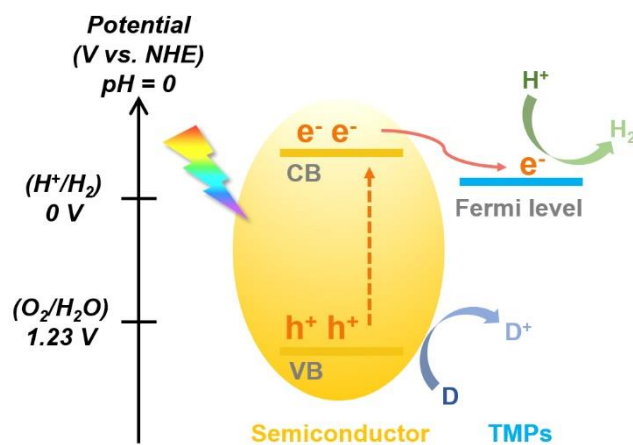


Fig. 3. Description of band diagram for photocatalytic H_2 production over a semiconductor photocatalyst loaded with TMPs cocatalyst.

Accepted MS

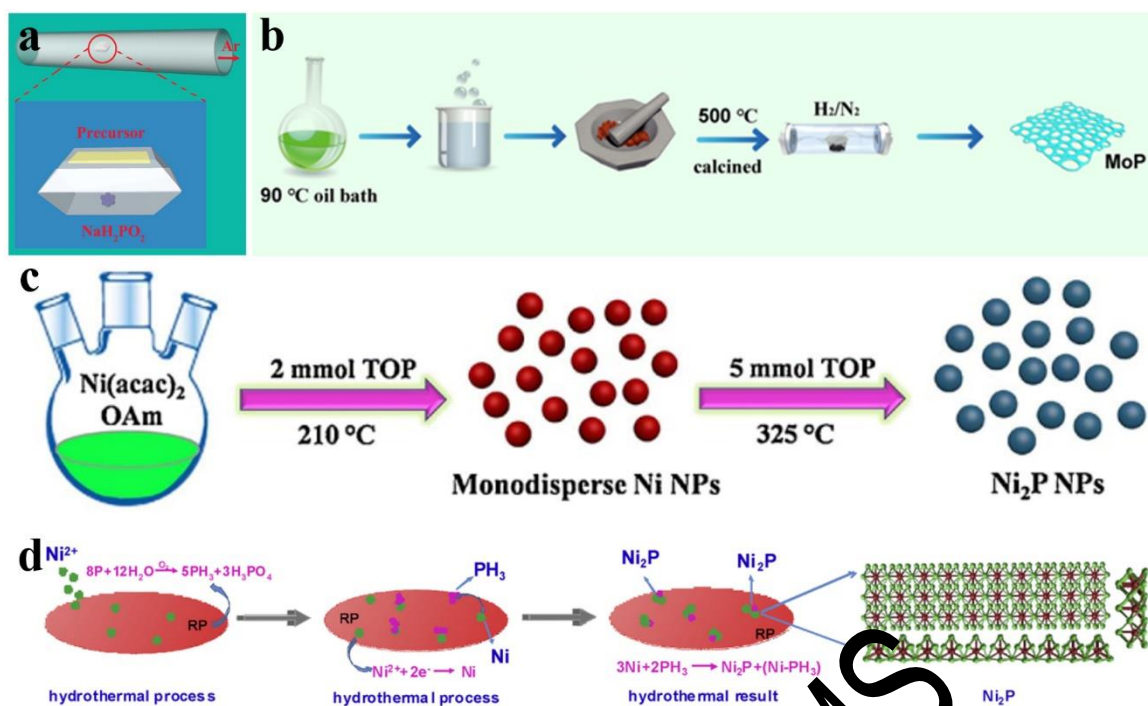


Fig. 4. (a) Schematic illustration of thermal phosphorization reaction. Reproduced with permission from Ref. [78] Copyright 2019 Royal Society of Chemistry. (b) Schematic synthesis of MoP. Reproduced with permission from Ref. [80] Copyright 2018 Elsevier. (c) Schematic synthesis of Ni_2P nanoparticles. Reproduced with permission from Ref. [82] Copyright 2018 Elsevier. (d) The possible formation mechanism process of $\text{Ni}_2\text{P}/\text{RP}$ the composite. Reproduced with permission from Ref. [85] Copyright 2019 Elsevier.

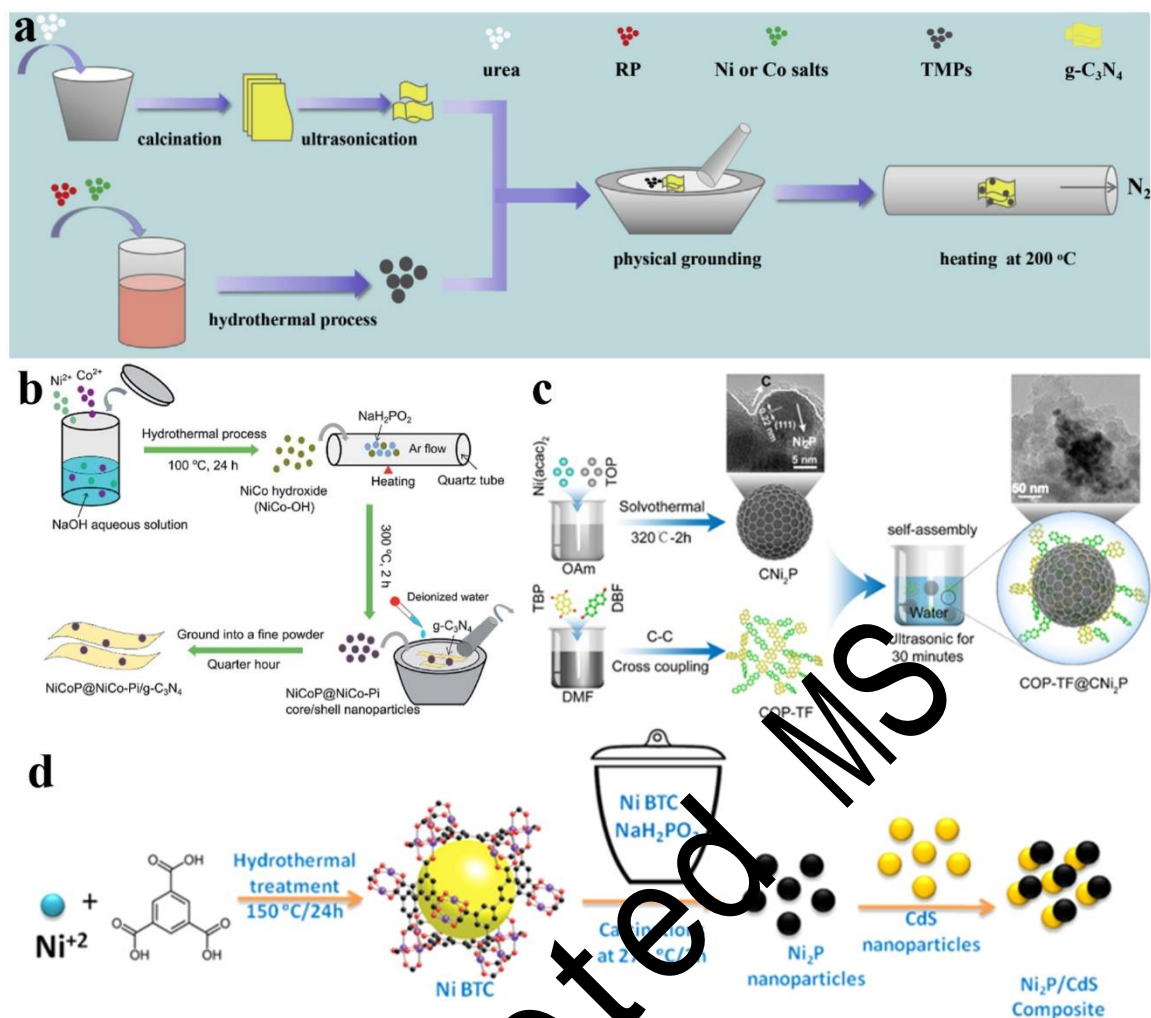


Fig. 5. (a) Schematic illustration of the formation of TMPs/g-C₃N₄ photocatalysts. Reproduced with permission from Ref. [89] Copyright 2019 Elsevier. (b) Schematic illustration for the fabrication of the NiCoP@NiCo-Pi/g-C₃N₄ photocatalyst. Reproduced with permission from Ref. [90] Copyright 2017 Royal Society of Chemistry. (c) Schematic illustration of the synthetic route of the hybrid photocatalyst COP-TF@CNi₂P. Reproduced with permission from Ref. [91] Copyright 2019 American Chemical Society. (d) Synthesis of Ni₂P/CdS Composite.

Reproduced with permission from Ref. [92] Copyright 2016 American Chemical Society.

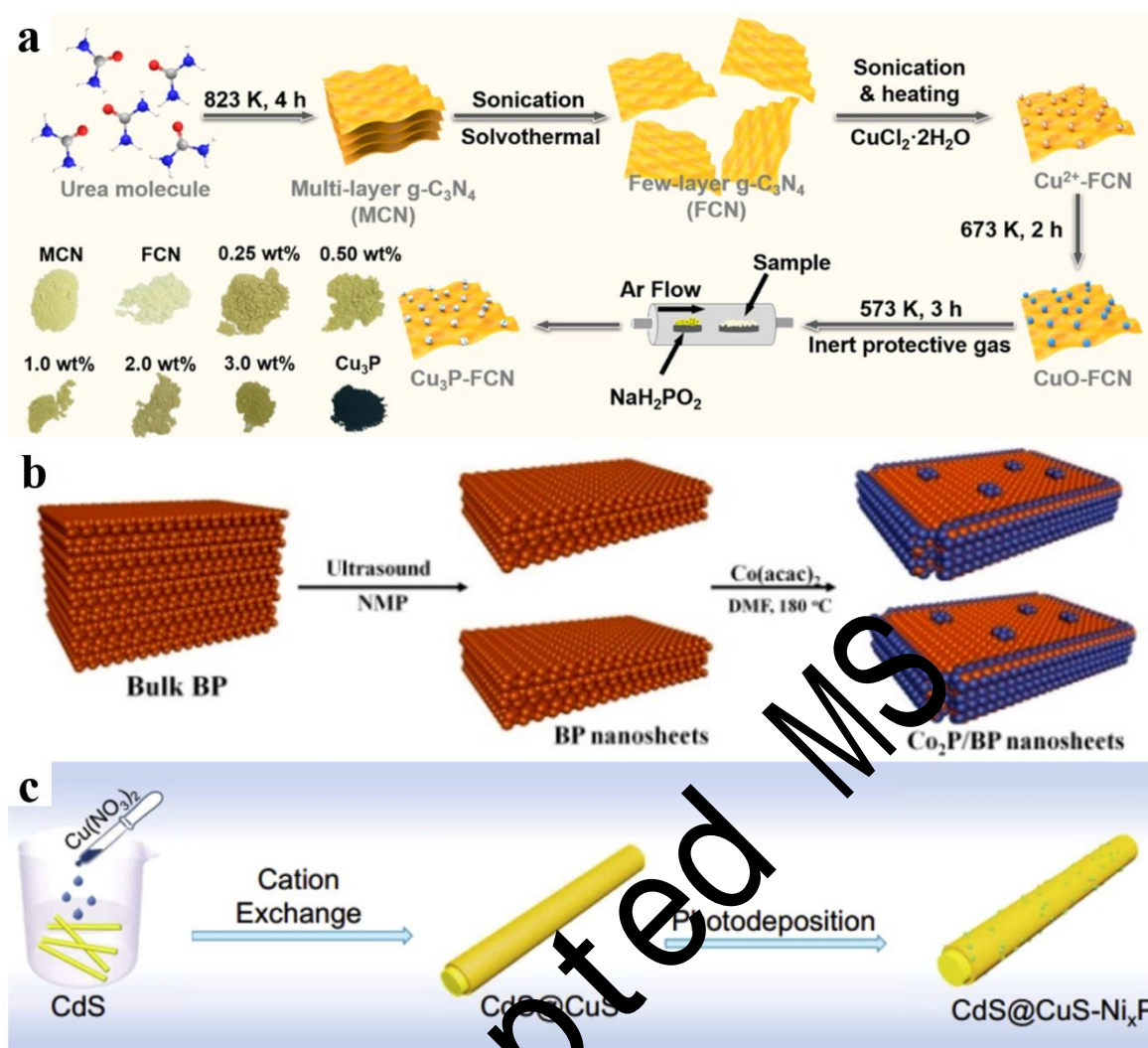


Fig. 6. (a) Synthetic procedures for the Cu_3P -FCN hybrids and digital photographs of the photocatalysts. Reproduced with permission from Ref. [13] Copyright 2019 American Chemical Society. (b) Schematic illustration for the preparation of Co_2P /BP nanosheets photocatalyst. Reproduced with permission from Ref. [77] Copyright 2019 American Chemical Society. (c) Schematic illustration of the synthesis of the $\text{CdS@CuS-Ni}_x\text{P}$ core-shell nanowires. Reproduced with permission from Ref. [96] Copyright 2019 Elsevier.

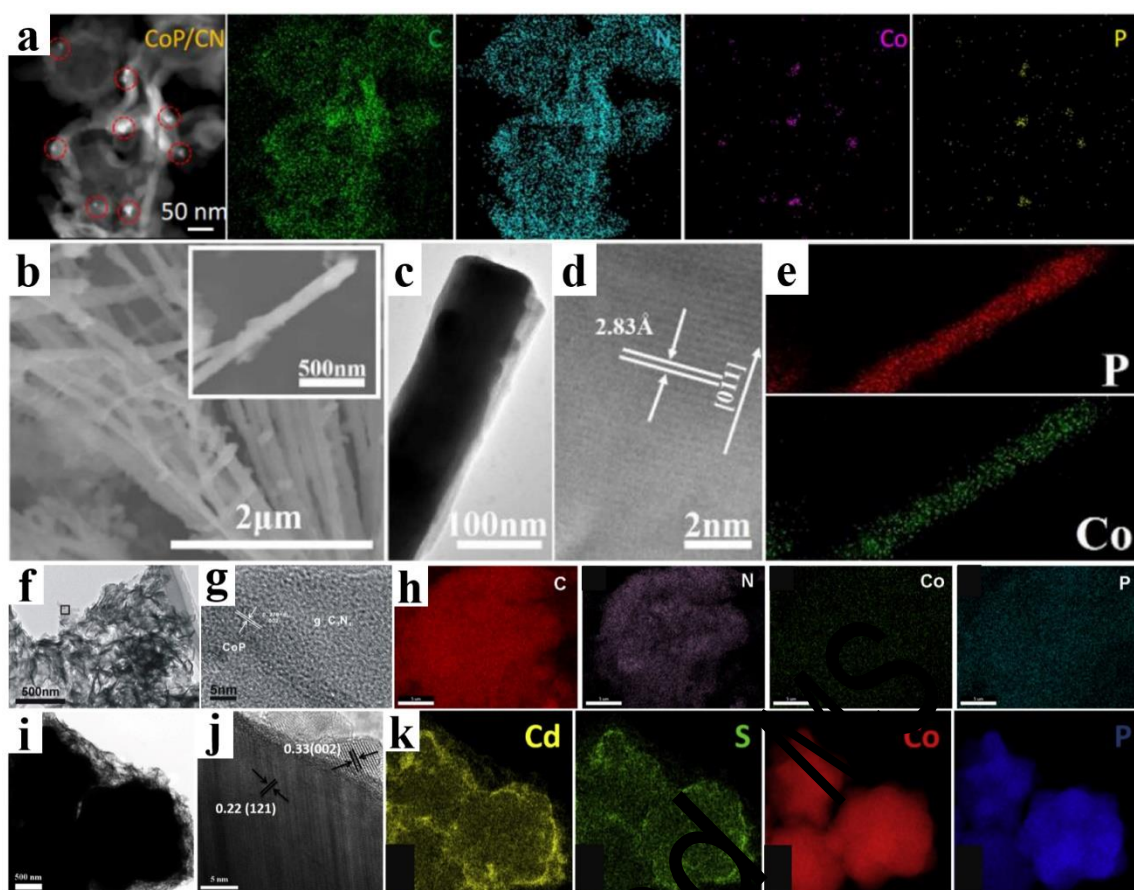


Fig. 7. (a) The TEM images and elemental mapping results of CoP/CN with element C, N, Co, and P. Reproduced with permission from Ref. [124] Copyright 2019 Elsevier. (b) SEM, (c) TEM, (d) HRTEM and (e) elemental mapping images of CoP nanowires. Reproduced with permission from Ref. [122] Copyright 2018 Elsevier. (f) TEM, (g) HRTEM and (h) SEM mapping images of 2%CoP/CN composite. Reproduced with permission from Ref. [62] Copyright 2018 Royal Society of Chemistry. (i) TEM, (j) HRTEM and (k) elemental mapping images of CdS-15/Co₂P microspheres. Reproduced with permission from Ref. [137] Copyright 2019 Elsevier.

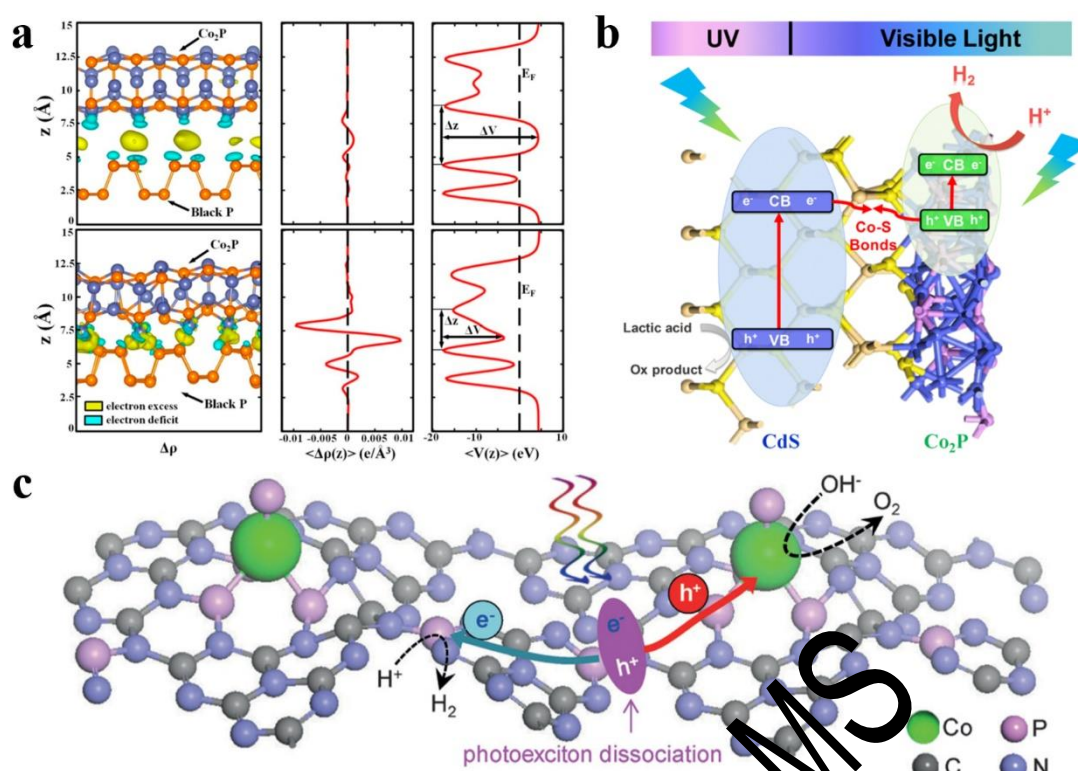


Fig. 8. (a) Electronic structure changes associated with assembling the Co₂P/BP heterojunction without (upper panel) and with (middle panel) chemical bonding from isolated layers. Reproduced with permission from Ref. [77] Copyright 2019 American Chemical Society. (b) Illustration of mechanism of Co₂P/CdS under UV-vis light irradiation. Reproduced with permission from Ref. [127] Copyright 2019 American Chemical Society. (c) Schematic illustration of the solar-driven overall water splitting on the Co₁-phosphide/PCN photocatalyst. Reproduced with permission from Ref. [130] Copyright 2017 Wiley.

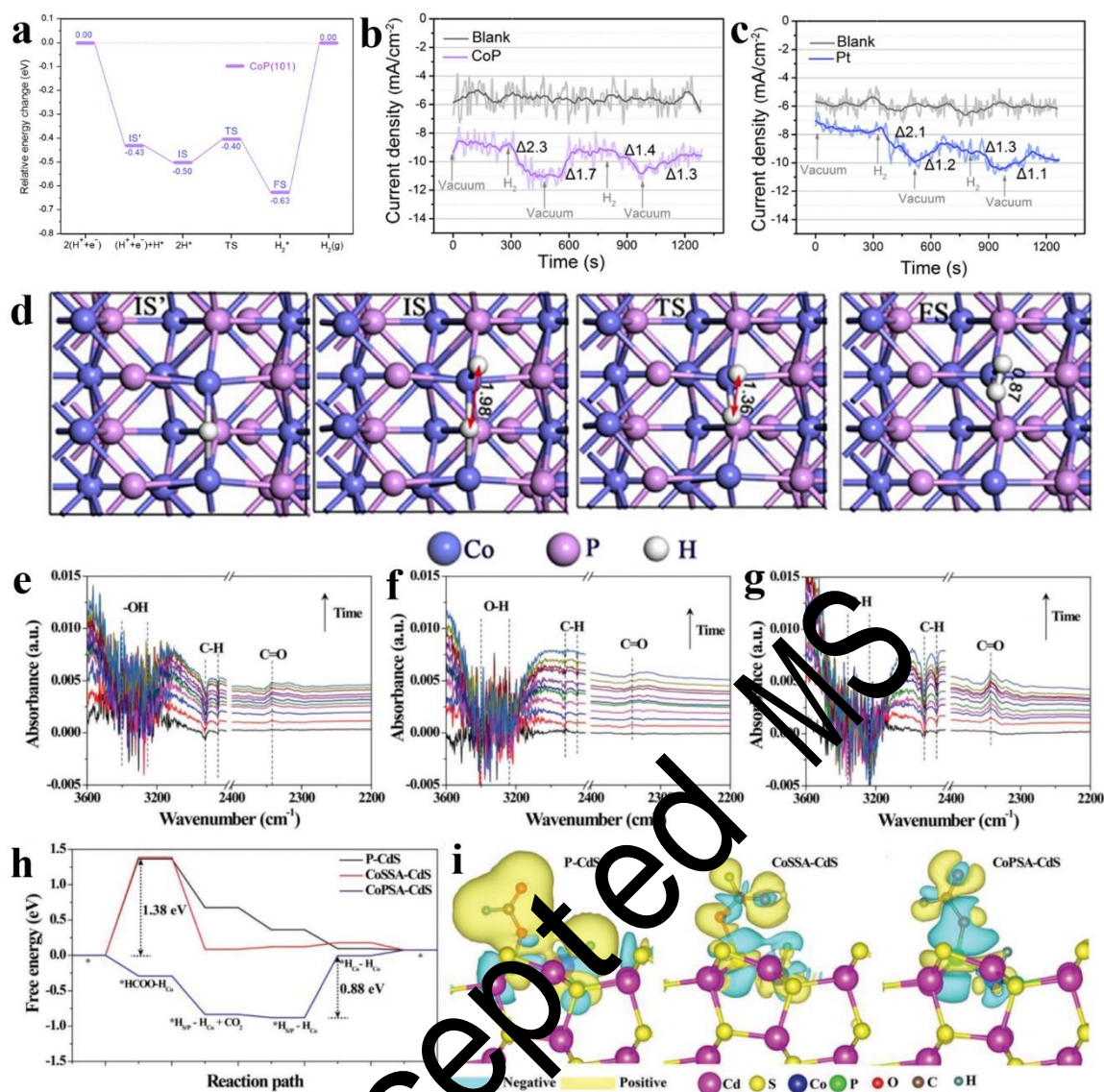


Fig. 9. (a) Calculated energy profile for hydrogen production on CoP (101) surface; Gas adsorption-desorption test for (b) CoP and (c) Pt coated electrode at 1 V; (d) The optimized structures of the initial states (IS), transition state (TS), and final state (FS), as labeled in (a). Reproduced with permission from Ref. [140] Copyright 2018 Elsevier. In situ IR spectrum analysis of the photocatalytic FA dehydrogenation over (e) P-CdS, (f) CoSSA-CdS and (g) CoPSA-CdS; (h) The calculated energy profile for FA dehydrogenation and hydrogen production on P-CdS, CoSSA-CdS and CoPSA-CdS; (i) The charge density difference maps between the adsorbed FA and CdS of P-CdS, CoSSA-CdS and CoPSA-CdS. Reproduced with permission from Ref. [141] Copyright 2019 Wiley.

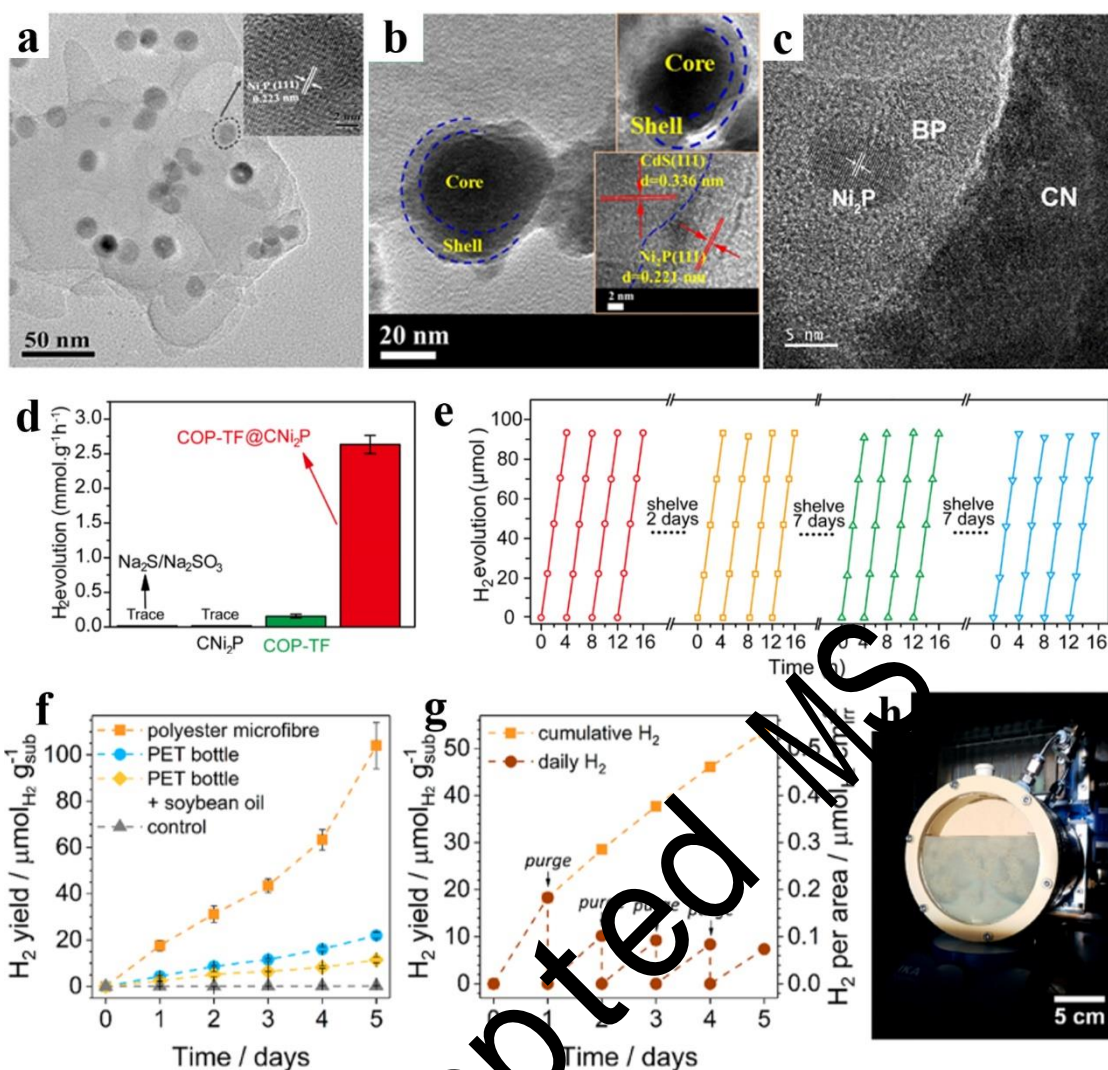


Fig. 10. (a) High-magnification TEM image along with HRTEM image (inset) of g-C₃N₄/3.5% Ni₂P. Reproduced with permission from Ref. [82] Copyright 2018 Elsevier. (b) HRTEM image of 10Ni₂P@CdS. Reproduced with permission from Ref. [68] Copyright 2018 Elsevier. (c) HRTEM image of Ni₂P@BP/CN. Reproduced with permission from Ref. [146] Copyright 2019 Elsevier. (e) Photocatalytic H₂ production ability of CNi₂P, COP-TF and COP-TF@CNi₂P samples; (f) Stability test of COP-TF@Ni₂P during photocatalytic H₂ production under seawater. Reproduced with permission from Ref. [91] Copyright 2019 American Chemical Society. (f) Long-term photoreforming of polyester microfibers, a PET bottle and an oil-coated PET bottle; (g) Upscaled photoreforming of polyester microfibers; (h) Photograph of the batch reactor in use. Reproduced with permission from Ref. [159]

Copyright 2019 American Chemical Society.

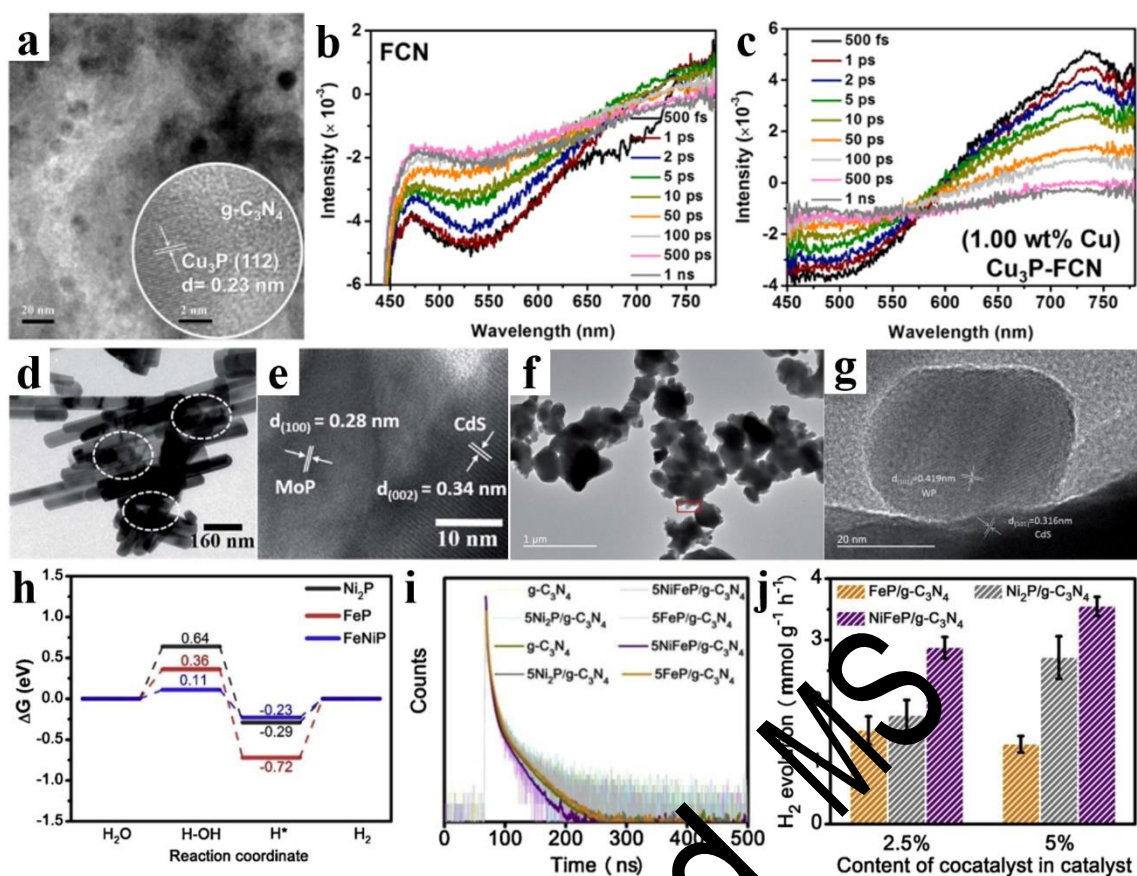


Fig. 11. (a) TEM and HRTEM (inset) images of Cu_3P -FCN. (b) UV-Vis spectra at various delay times of (b) FCN and (c) Cu_3P -FCN. Reproduced with permission from Ref. [163] Copyright 2019 American Chemical Society. (d) TEM and (e) HRTEM images of MoP/CdS nanorods. Reproduced with permission from Ref. [169] Copyright 2015 Royal Society of Chemistry. (f) TEM and (g) HRTEM images of WP/CdS. Reproduced with permission from Ref. [170] Copyright 2017 Royal Society of Chemistry. (h) Free energy diagrams for H_2O reduction to H_2 by the thermochemical model on Ni_2P , FeP and NiFeP surface; (i) Time-resolved fluorescence decay spectra of the samples; (j) Photocatalytic H_2 production rates of $\text{FeP/g-C}_3\text{N}_4$, $\text{Ni}_2\text{P/g-C}_3\text{N}_4$ and $\text{NiFeP/g-C}_3\text{N}_4$. Reproduced with permission from Ref. [177] Copyright 2019 Elsevier.